

Radiomics and artificial intelligence for precision medicine in lung cancer treatment

Mitchell Chen ^{a,b}, Susan J. Copley ^{a,b}, Patrizia Viola ^c, Haonan Lu ^a, Eric O. Aboagye ^{a,*}

^a Department of Surgery and Cancer, The Commonwealth Building, Du Cane Road, Hammersmith Campus, Imperial College, London W12 0NN, UK

^b Imperial College Healthcare NHS Trust, Hammersmith Hospital, Du Cane Road, London W12 0HS, UK

^c North West London Pathology, Charing Cross Hospital, Fulham Palace Rd, London W6 8RF, UK



ARTICLE INFO

Keywords:

Lung cancer
Radiomics
Radiogenomics
Artificial intelligence
Precision medicine

ABSTRACT

Lung cancer is the leading cause of cancer-related deaths worldwide. It exhibits, at the mesoscopic scale, phenotypic characteristics that are generally indiscernible to the human eye but can be captured non-invasively on medical imaging as radiomic features, which can form a high dimensional data space amenable to machine learning. Radiomic features can be harnessed and used in an artificial intelligence paradigm to risk stratify patients, and predict for histological and molecular findings, and clinical outcome measures, thereby facilitating precision medicine for improving patient care. Compared to tissue sampling-driven approaches, radiomics-based methods are superior for being non-invasive, reproducible, cheaper, and less susceptible to intra-tumoral heterogeneity. This review focuses on the application of radiomics, combined with artificial intelligence, for delivering precision medicine in lung cancer treatment, with discussion centered on pioneering and groundbreaking works, and future research directions in the area.

1. Introduction

Lung cancer is the leading cause of cancer-related deaths worldwide. In 2020, there were 2.2 million new cases and 1.8 million deaths globally, corresponding to 21% of all cancer-related mortality [1]. With its high prevalence and mortality, lung cancer poses a significant health challenge. Lung cancer can arise from various sites in the bronchial architecture, leading to varied initial clinical presentation, ranging from being asymptomatic to presenting with haemoptysis and cachexia. Lung

cancer symptomatology, if any, is non-specific, resulting in over 70% of patients being diagnosed when the disease is already in an advanced stage (International Association for the Study of Lung Cancer (IASLC) stage III or IV) [2]. This contributes to its poor mean 5-year survival rate of 20–30% [3].

Lung cancer is a heterogeneous disease entity with a range of histological subtypes and growth patterns. Non-small cell lung cancer (NSCLC) is the predominant histological type, accounting for 80–85% of all lung cancer cases [4]. Of these, squamous cell carcinoma (SCC) has

Abbreviations: IASLC, International Association for the Study of Lung Cancer; NSCLC, Non-Small Cell Lung Cancer; SCC, Squamous Cell Carcinoma; AdC, Adenocarcinoma; AIS, Adenocarcinoma In Situ; MIS, Minimally Invasive Adenocarcinoma; NSCLC-NOS, NSCLC - Not Otherwise Specified; TTF-1, Thyroid Transcription Factor - 1; IHC, Immunohistochemistry; SCLC, Small Cell Lung Cancer; SBRT, Stereotactic Beam Radiotherapy; TME, Tumoral Microenvironment; PD-1, Programmed Cell Death 1; PD-L1, Programmed Cell Death Ligand-1; qRT-PCR, Quantitative reverse transcriptase polymerase chain reaction; CBI, Checkpoint Blockade Immunotherapy; ROI, Region of Interest; ICC, Intra-class Correlation Coefficient; FDG, ¹⁸F-fluorodeoxyglucose; IBSI, Image Biomarker Standardisation Initiative; GLCM, Gray-Level Co-Occurrence Matrix; RQS, Radiomics Quality Score; TRIPOD, Transparent Reporting of a multivariable prediction model for Individual Prognosis Or Diagnosis; AUROC, Area under the Receiver Operating Characteristic Curve; PET, Positron Emission Tomography; CT, Computed Tomography; MTV, Metabolic Tumour Volume; SUN_{max}, Maximum Standard Uptake Value; FDR, False Detection Rate; RPV, Radiomics Prediction Vector; CNN, Convolutional Neural Network; CI, Confidence Interval; TCIA, The Cancer Imaging Archive; GSEA, Gene Set Enrichment Analysis; scRNAseq, Single-Cell RNA sequencing; TKI, Tyrosine Kinase Inhibitor; EGFR, Epidermal Growth Factor Receptor; FGFR1, Fibroblast Growth Factor Receptor 1; KRAS, Kirsten Rat Sarcoma viral oncogene; PIK3CA, Phosphatidylinositol-4,5-bisphosphate 3-kinase, Catalytic subunit Alpha; HER2, Human Epidermal Growth factor receptor 2; BRAF, v-RAF murine sarcoma viral homolog B1; ALK, Anaplastic Lymphoma Kinase; NTRK, Neurotrophic Tyrosine Receptor Kinase; OS, Overall Survival; RFS, Recurrence-Free Survival; CTLA4, Cytotoxic T-cell Lymphocyte Antigen 4; cfDNA, Plasma-derived Cell Free DNA; ddPCR, Digital Droplet Polymerase Chain Reaction.

* Correspondence to: Cancer Imaging Cancer, Department of Surgery and Cancer, Room GN1 Commonwealth Building, Du Cane Road, Hammersmith Campus, Imperial College, London W12 0NN, UK.

E-mail address: eric.aboagye@imperial.ac.uk (E.O. Aboagye).

<https://doi.org/10.1016/j.semcancer.2023.05.004>

Received 2 December 2022; Received in revised form 14 April 2023; Accepted 17 May 2023

Available online 19 May 2023

1044-579X/© 2023 The Author(s). Published by Elsevier Ltd. This is an open access article under the CC BY-NC-ND license (<http://creativecommons.org/licenses/by-nc-nd/4.0/>).

the strongest link to tobacco smoking and the tendency to cavitate; they are more likely to arise from the main bronchi and propagate towards the carina. Adenocarcinoma (AdC) is the most common NSCLC subtype; it usually originates more peripherally and compared to other subtypes, has more specific growth patterns and molecular characteristics. In 2011, IASLC introduced the current classification system for AdC, where the disease is subdivided into adenocarcinoma in situ (AIS), minimally invasive adenocarcinoma (MIS) and invasive adenocarcinoma, depending on tumour size, histological growth pattern and degree of stromal invasion [5]. AIS and MIA are generally indolent tumours that can be effectively treated with surgical resection, with no risk of recurrence at 5 years [6], whereas invasive adenocarcinoma, particularly the mucinous type demonstrating micropapillary growth pattern, is associated with aggressive spread and poorer prognoses [7]. Large cell carcinomas, or NSCLC not otherwise specified (NSCLC-NOS), negative for thyroid transcription factor-1 (TTF1) and p40 on immunohistochemistry (IHC) and lack the squamous or glandular morphology observed in the first two NSCLC subtypes, are typically more centrally located with a tendency for mediastinal invasion. Small cell lung cancers (SCLC) account for 10–15% of lung cancer cases and arise from the neuroendocrine cells of the bronchial mucosa [8]. As with NSCLC-NOS, they tend to present as central/mediastinal neoplasms with highly aggressive features. Although a common staging system (IASLC 8th edition) is used for all lung cancers, treatment varies depending on tumour histology, because of the differences in their characteristic progression pattern and prognosis.

Evidence supports the early detection and treatment of lung cancer, prompting the adoption of screening programmes for high-risk patients in certain countries [9,10]. The treatment options for early-stage lung cancer include surgical resection, stereotactic beam radiotherapy (SBRT), and percutaneous ablation, depending on patient's preference, preserved lung function and suitability for surgery. The mainstay for treating unresectable NSCLC is traditionally chemoradiotherapy [11]. It has limited efficacy however, and significant side effects [12]. Newer treatment options such as driver mutation targeting therapy and checkpoint blockade immunotherapy (CBI) have redefined the landscape for NSCLC management. However, their high treatment failure rates, combined with higher costs and associated complications, call for better ways of patient selection. The current practice of selecting patients for these treatments is by histological sampling of the tumour through percutaneous lung biopsy, endobronchial biopsy, or surgical resection, followed by molecular testing for driver mutations, and/or immunohistochemical staining of the sample to measure the percentage of cancer cells expressing the inhibition target receptor such as programmed cell death ligand 1 (PD-L1) [13]. Tumour-infiltrating immune cell sampling from biopsies, however, suffers from significant sampling variation due to intra-tumoral heterogeneity, so the sampled tissue might not be representative of the rest of the tumour [14]. Additionally, repeated biopsies might be needed, as driver mutations and receptor expression can evolve over time [5]. Finally, the process of tissue sampling itself can be hindered by patient tolerance, procedural complications, and the quantity and quality of tissues obtained [15].

In lung cancer diagnosis and work-up, anatomic (CT) and molecular imaging (PET-CT) are routinely acquired to radiologically evaluate the tumour. Clinical radiologists utilise these data to characterise and stage the disease, based on pattern recognition skills developed through their training and clinical experience. This information is combined with histological and molecular findings to aid in treatment planning. In radiological practice, imaging features, other than size measurements, are descriptive and qualitative in nature. The quantitative aspect of the imaging data can be better captured by radiomic features, which are first or higher order metrics that form an active field of study in computational medical imaging. They convey disease information at the mesoscopic scale, that are generally indiscernible to human eye [16,17]. Lung cancer, particularly NSCLC, presents an ideal opportunity for radiomics because of the high contrast between the tumour and surrounding lung

parenchyma on imaging (CT and PET), good data availability owing to a high disease incidence rate and detection via screening programmes, and implications for improving treatment outcomes.

Following their extraction, radiomic features can be used in a statistical or deep learning paradigm to develop models predictive of various clinical outcomes. Since its inception, lung cancer radiomics has generated substantial research interest, with many published studies presenting models predicting tumour histology, presence of driver mutations, treatment response, adverse effects, post-treatment recurrence and patient prognosis, for a range of treatment options. More than 70% of such publications have been in the last three years, demonstrating a growing interest in the field (Fig. 1A).

Numerous review papers have been published in recent years on the application of radiomics to lung cancer treatment. A bibliometric search revealed 55 such reviews published in the last three years (Fig. 1B). Most of these were either primers on radiomics to a clinical audience, or focused reviews of published literature on a specific type of lung cancer treatment. There has been limited coverage of radiomics in terms of their significance to understanding cancer biology.

In this review, we present the concept and key feature classes of radiomics, their integration with machine learning methods for developing models predictive of tumour histology and clinical outcomes and discuss how they can contribute to advancing our understanding of the disease at the molecular and cellular levels.

2. Radiomics

2.1. Introduction

The suffix “-omics” is widely used in biomedical disciplines to denote the extraction of valuable information from a large dataset. Radiomics pertains to the extraction of quantitative information from medical imaging data.

The earliest application of radiomics can be traced back to a study demonstrating the correlation of patient's time-to-progression with energy feature in lung cancer [18] and another by Segal et al. deriving twenty-eight imaging traits that can reconstruct 78% of the global gene expression profiles, revealing cell proliferation, liver synthetic function, and patient prognosis [19]. The concept gained significant traction following a landmark publication by P. Lambin [20], who formally coined the term in the context of cancer treatment.

2.2. Radiomic features

Radiomics encompasses several feature classes, ranging from first order ones such as energy and entropy to higher order features such as those derived from wavelet and Laplacian of Gaussian filtered data. The Image Biomarker Standardization Initiative (IBSI) [21] was established to publicise a list of radiomic features with proven reproducibility. The IBSI compliant features that are computable using the open-source package Pyradiomics [22] are presented as phylogenetic tree in Fig. 2A.

2.2.1. Shape

Shape features capture information on the two or three-dimensional geometry of the objects of interest and include measurements such as maximal or minimal diameters and total volume, as well as the ratios of maximal to minimal diameter, and surface to volume. In the context of lung cancer imaging, tumour size, as measured by simple diameter or volumetry, is a direct or surrogate measure of tumour T stage, a determinant of best treatment option and disease prognosis. Shape features can also determine the likelihood of a solitary pulmonary nodule being malignant, by assessing whether it's round or polygonal, or if there is spiculation. For example, a spherical nodule would have a smaller maximal to minimal diameter ratio, or higher compactness than one that is flat; the latter being a feature of nodule benignity [23]. Similarly, a tumour with smooth margin would have a lower surface to volume ratio

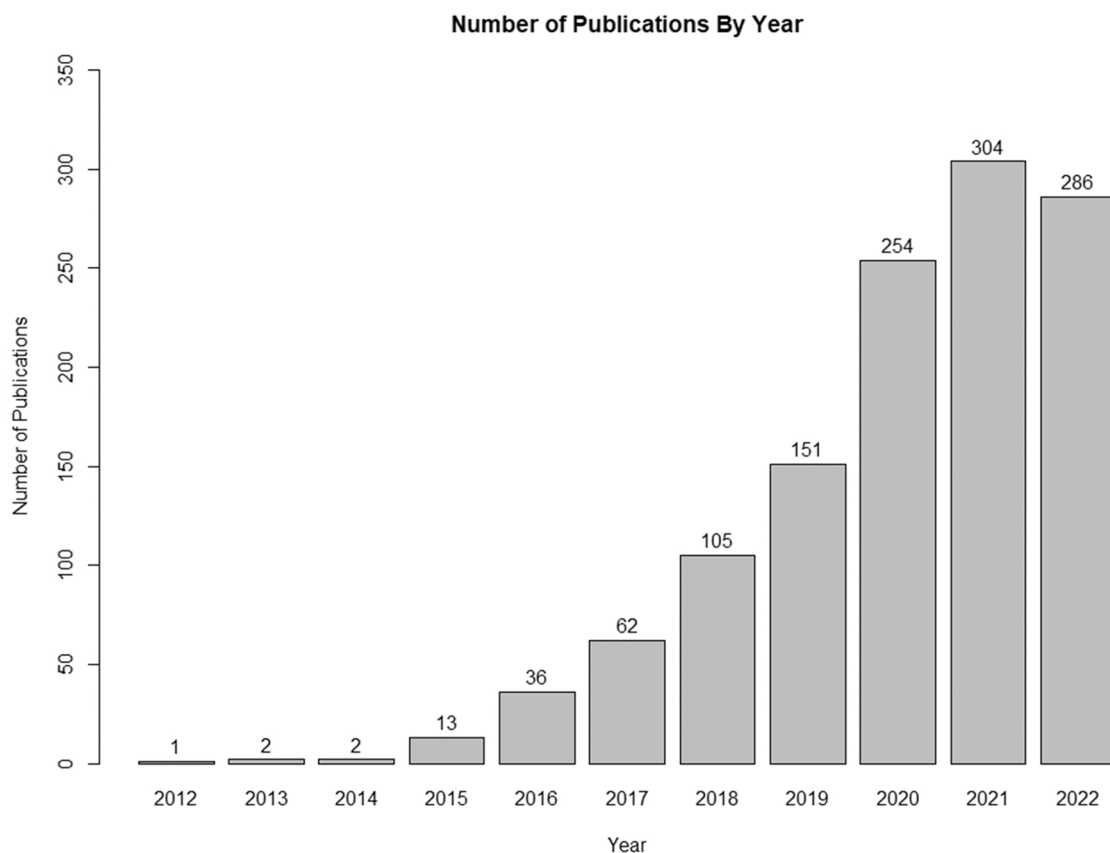
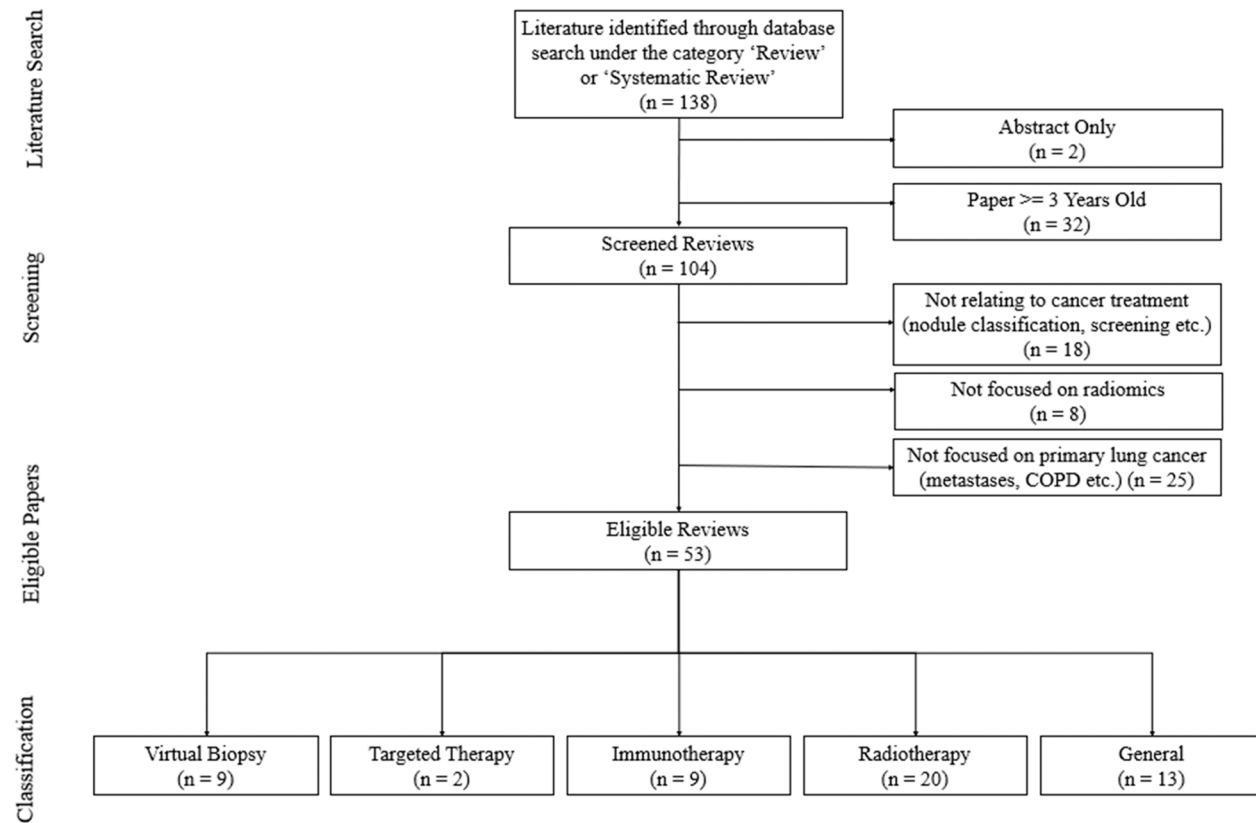
A**B**

Fig. 1. Trends in lung cancer radiomics research. A. Number of publications (March 2012 - October 2022 inclusive) on PubMed with the keywords "lung cancer" and "radiomics". Note more than 70% of these have been published in the last three years. B. Bibliometric search flowchart based on the search strategy in Fig. 1A, but for review papers on lung cancer treatment radiomics.

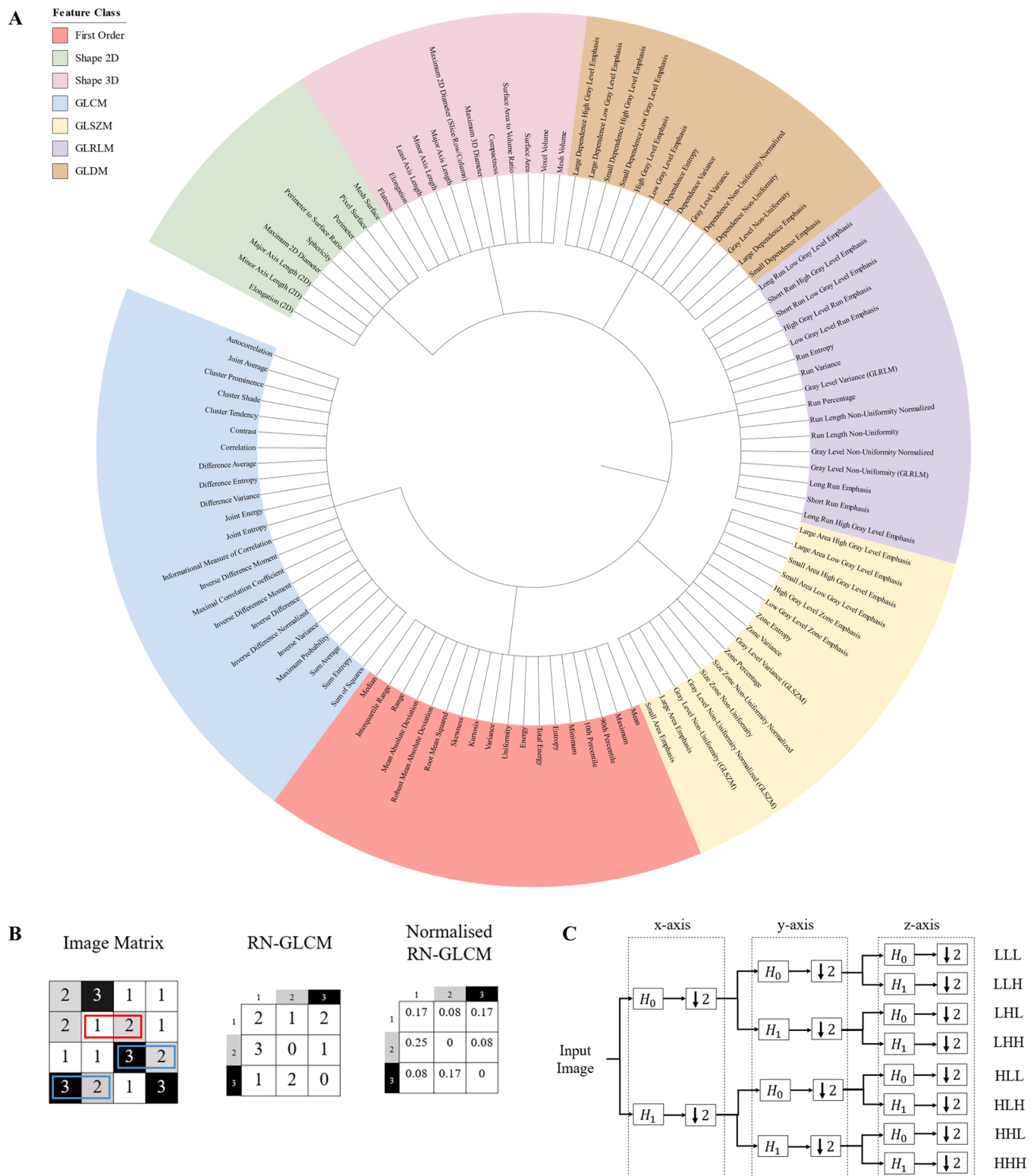


Fig. 2. Common radiomic features. A. Phylogenetic tree illustrating common radiomic features grouped by their class. Features listed are those computable using PyRadiomics and compliant with the Image Biomarker Standardization Initiative (IBSI). Highly correlated features such as sphericity, compactness and spherical disproportion, or standard deviation and variance, are omitted. B. Computation of right neighbour GLCM (RN-GLCM), by counting the number of qualifying pairs of pixels values and then normalising against the overall sum. The [1,2] pair is shown in red, and [2,3] pairs are in blue. This forms the basis of texture features. C. Decomposition of input image by applying wavelet transform in each axis. L and H represent low and high pass filters, respectively, followed by a downsampling step by a factor of two. The resulting transformed volumes are then calculated for a range of features.

than one with spiculation, which is again, a strong indicator of benignity [24].

2.2.2. Intensity

Intensity-based features include descriptive statistics of intensity distribution such as range, mean, median, variance, skewness or kurtosis. In CT radiomics, these would be derived from the radiodensity distribution of the region of interest (ROI), which could in turn be influenced by contrast phase and enhancement. In PET radiomics, they would be related to the uptake of [18] F-fluorodeoxyglucose (FDG) tracer. These features can facilitate a distinction between ground glass and solid tumoral components, or a measurement of enhancement or avidity, thereby determining the malignant potential of a lesion [25].

2.2.3. Texture

Texture features assess connectivity between voxels in a region of interest. The concept of quantifiable texture features on images has its roots in the study of aerial imagery of landscape in the 1970s [26]. In their study, Haralick et al. proposed a series of features that can measure the image texture and determine the type of land use that is being represented. These features are based on a building block known as grey-level co-occurrence matrix (GLCM). GLCM is determined by counting the number of pre-defined neighbours in a number-index pair and then normalised over the sum of elements (Fig. 2B).

The normalised GLCM can subsequently be used to compute texture features such as homogeneity, contrast, entropy and energy using the equations given in Table 1.

The homogeneity and contrast denote the level of uniformity and contrast of the image, respectively. Entropy measures complexity of texture: with a higher value present when the image textures are more random than regular. Energy measures the strength of textures present. Texture features can evaluate intra-tumoral heterogeneity, which reflects the presence of clonal subpopulations that drive tumour growth and the development of resistance to treatment [27].

2.2.4. Wavelet and Laplacian of Gaussian filters

Wavelet transformation provide higher order features computed by first decomposing a three-dimensional ROI into eight volumes using wavelet transformation, labelled such that LLH denotes a low pass filter was applied in the x- and y-axes and a high pass filter in the z-axis (Eq. (1) and Fig. 2C). For each decomposed volume, the texture features can then be computed to capture more complex texture patterns. For example, *GLCM_HHH* and *grey-level non-uniformity HLH* features have been found to be related to intra-tumoral heterogeneity in lung cancer, and *GLCM_LLH* to z-axis homogeneity and in-slice heterogeneity [28].

$$\begin{aligned} V^3 &= (L^x \oplus H^x) \otimes (L^y \oplus H^y) \otimes (L^z \oplus H^z) \\ &= L^x L^y L^z \oplus L^x H^y L^z \oplus H^x L^y L^z \oplus H^x H^y L^z \oplus L^x L^y H^z \oplus L^x H^y H^z \oplus H^x L^y H^z \\ &\quad \oplus H^x H^y H^z \end{aligned} \quad (1)$$

where H^i and L^i denote high and low pass filters passed along the i -axis, and \oplus and \otimes direct sum and convolution operators, respectively.

Through decomposition, the imaging data are separated into high

Table 1
Sample GLCM-based texture features.

Feature	Equation	Meaning
Homogeneity	$\sum_{ij} \frac{GLCM(i,j)}{1 + (i-j)^2}$	Homogeneity of pixel values
Contrast	$\sum_{ij} GLCM(i,j)(i-j)^2$	Difference between neighbouring pixels
Entropy	$\sum_{ij} GLCM(i,j) \log GLCM(i,j)$	Disorder/complexity of image texture
Energy	$\sum_{ij} GLCM(i,j)^2$	Textural strength

and lower frequency domains, enriching image heterogeneity and homogeneity, respectively [29]. Subsequently computing the texture features in the split channels allows for a targeted quantification of tumour characteristics. For example, *HHH_GLCM* family features highlight tumour boundary and internal tumour homogeneity, while *LLH_GLCM* highlights z-axis homogeneity and in-plane heterogeneity. These direction-specific measurements can be particularly useful in capturing the characteristics of cancers demonstrating a lung architecture-dependent growth pattern, such as growth propagating along the peribronchovascular bundle or limited by pulmonary fissures.

Laplacian of Gaussian is another spatial image filter that can be applied, by convolving the imaging data with the second derivative of a Gaussian kernel. This can reduce image noise and helps the derived features to better find intensity edges and highlight regions of rapid change, which have been shown to differentiate between tumour subtypes [77].

Features derived from wavelet or Laplacian of Gaussian filtered data do not currently form part of IBSI but are being reviewed for potential inclusion in a later edition [21].

2.3. Workflow

The standard workflow for model development begins with data curation, which involves ensuring the consistency of certain image data characteristics such as scan acquisition parameters and contrast enhancement. Unsatisfactory data are excluded from the model development process. Variations in scanner make, model, spatial resolution and peak kilovoltage are generally acceptable for images acquired on modern scanners. A pre-processing step would be applied to homogenise voxel size through up- or down-sampling, following by standardisation of the voxel intensity to a mean of zero and standard deviation of unity.

2.3.1. Feature extraction

Several open-source and proprietary software packages are available for automated feature extraction, most notably PyRadiomics [22], which offers an integrated data pre-processing step, batch extraction option, and a 3D Slicer plug-in to facilitate operation via a graphical user interface [30].

2.3.2. Feature redundancy and reproducibility

Up to 1500 features can be extracted by PyRadiomics per image, some of which present overlapping information. The inclusion of such features can introduce unnecessary bias to model development and increase the risk of overfitting [31]. Examples include intensity features such as standard deviation and variance, and shape features such as spherical disproportion and sphericity.

Not all feature redundancies are as conceptually appreciable. More intricate redundancies can be identified and reduced using consensus clustering [32,33], where the feature space is reduced into several non-redundant feature clusters, by maximising the correlation of features within each cluster.

Feature reproducibility is another important issue to address, particularly with varied image acquisition, reconstruction and segmentation [34]. Depending on its source, feature reproducibility can be ascertained using test-retest, repeated scan acquisition or multi-observer segmentation techniques. Intra-class correlation coefficient (ICC) would be calculated (Eq. (2)) [35], with features below a certain threshold (typically 0.75–0.90) rejected.

$$ICC = \frac{\text{Between subject variance}}{\text{Between subject variance} + \text{Within subject variance}} \quad (2)$$

Finally, predictive models are usually composite vectors of weighted features. Therefore, reproducibility of the vector, not just individual features, should also be considered.

2.3.3. Feature standardisation

In 2020, IBSI introduced a list of 169 features with standard definitions and proven reproducibility. Expert consortia have issued guidelines for conducting radiomics research, the compliance to which can be assessed as the Radiomics Quality Score (RQS) [17]. The Transparent Reporting of a multivariable prediction model for Individual Prognosis or Diagnosis (TRIPOD) statement presents reporting guidelines which cover most radiomics-based studies [36].

2.3.4. Feature harmonisation

In features computed from data pooled from multiple centres, variations in scanner and image acquisition parameters can give rise to undesirable batch effect, affecting model performance. This calls for feature harmonisation. A well-known harmonisation technique in radiomics is ComBat [37], which has been shown to reduce diverging feature distributions in a lung cancer dataset scanned on six different imaging protocols to less than 2%. [38] Newer ComBat methods have since been proposed, with BM-ComBat reporting the best performance [38].

2.4. Segmentation

2.4.1. Multi-region radiomics

The earliest studies of lung cancer radiomics were based on radiomic features extracted from a single ROI, namely one that is contoured around the tumour [39,40]. However, this approach omits the peritumoral area, where rich information on tumoral growth and microenvironment (TME) are believed to be contained. For example, in clinical radiology, peripheral ground glass changes are thought to represent tumoral changes at the upper limit of the spatial resolution of CT. In ADC, this feature is classically associated with lepidic growth on histology; the literature has reported peripheral ground glass opacity to be associated with a more favourable prognosis, irrespective of the histological growth pattern that it represents [41]. Background lung parenchyma distant to the primary tumour presents yet another source of potentially valuable information, given the higher risk of carcinogenesis in lung areas affected by emphysema and fibrosis [42].

In multi-region radiomics, features are extracted from these additional ROIs, as shown in Fig. 3A, for a more comprehensive analysis of the disease, and making distinctions between features from different ROIs. The latter could help with model interpretation, when correlating retained radiomic features with histological and radiological findings.

Multi-region radiomics is becoming the mainstay of lung cancer radiomics in recent literature [43–45].

2.4.2. Tumour segmentation

Traditionally, the tumour ROIs are contoured manually on CT, usually by more than one clinically trained observer to offset the impact of observer bias. In recent years, however, machine learning, particularly deep learning, has greatly accelerated the workflow of lung cancer radiomics. In the latest studies, tumour segmentation is performed either semi-automatically, assisted by methods such as GrowCut where user-defined seeds are placed to guide segmentation [46], or full-automatically using convolutional neural network-based methods, such as PHISeg [47], and nnUNet. [48].

By limiting human input into the process, observer variability is controlled. For this reason, automated segmentation is favoured for its superior reproducibility [49]. However, against the backdrop of this benefit, a fully automated segmentation could be challenged for its clinical validity and might be less accurate where the tumour abuts anatomical structures with similar radiodensity (eg. pleura, collapsed lung, traversing vasculature etc.). At this stage, ROI validation by expert readers remains relevant, and should continue to be incorporated into the standard pipeline for radiomics. Machine learning methods can, however, greatly speed up the validation process by minimising the amount of user interaction required.

On PET, tumour segmentation can be achieved by finding the metabolic tumour volume (MTV) based on a relative uptake threshold, such as 40% of the maximum standard uptake value, SUV_{max} . There is currently no consensus on the optimal threshold for lung cancer radiomics, with MTV30 or MTV40 being the most adopted thresholds [50].

2.5. Model development

Following segmentation, pre-processing, feature extraction and normalisation, a high dimensional, high throughout dataspace is formed.

The development or *discovery cohort* is divided into a *training* and *internal validation set*, balanced for relevant patient factors such as patient age, performance status and cancer stage. The *training set* is then used for model training, and *internal validation set* used for determining the optimal training parameters. The optimal dimensionality reduction and regularisation choices can be determined based on the best observed performance on the *internal validation set*. (Fig. 3G).

Model development can be powered by statistical or deep learning. In statistical learning, this begins with dimensionality reduction. An initial regression-based step can be applied to eliminate non-significant features with a false detection rate (FDR) above a pre-defined threshold (usually 5%), which could be based on logistic regression for a binary outcome such as treatment response, or Cox regression for survival prediction. This can be followed by correlation analysis to identify and exclude inter-correlated features.

Various statistical and machine learning algorithms have been utilised for model development in lung cancer radiomics (Table 2), some for further dimensionality reduction and others combined with model construction in an embedded framework.

In parametric modelling, a functional form is assumed. For linear regression, this would follow Eq. (3).

$$RPV = \beta_1x_1 + \beta_2x_2 + \dots + \beta_nx_n \quad (3)$$

where the radiomics prediction vector (RPV) is a sum of features $x_1 \dots x_n$ with weights $\beta_1 \dots \beta_n$. For the prediction of binary or survival outcomes, logistic or Cox regression model is used, respectively. Naïve Bayes (NB) is a parametric classifier that calculates probabilistic priors and uses Bayesian statistics to predict the outcome. It has the advantage of requiring smaller training samples to attain good performance but is limited by its assumption of independence of features [51].

For a more general approach without the functional form assumption, studies have investigated the use of various non-parametric methods [52,53]. K-nearest neighbours (KNN) works by minimising the spatial distance from the plane of separation to the nearest datapoints. It is free from the feature independence assumption of NB, but is prone to overfitting, which is particularly problematic in a large feature space such as that of radiomics. [54] Random forest (RF) is based on a trained ensemble of decision trees, achieved through bootstrap aggregation. Like KNN, RF is also susceptible to overfitting [55]. Support vectors machine (SVM) computes the hyperplane that separates the datapoints, aided by kernel trick transformation when they are not directly separable [56]. Comparing to their parametric counterparts, non-parametric models are generally limited in their interpretability and the scope for inference as well as being susceptible to a deterioration in performance in the high dimensional space (the so-called “curse of dimensionality”) [57]. One classifier benchmarking study demonstrated superior performance of NB to RF and KNN when applied to the same dataset for predicting lung cancer histology, a finding attributed to the sensitivity of the latter two to noise [58]. In a separate benchmarking study for patient prognostication using PET-CT radiomics, RF showed marginally better predictive performance than SVM, logistic regression and tumour staging, though no comparison to other parametric methods was made [59].

The above methods achieve feature selection based on training

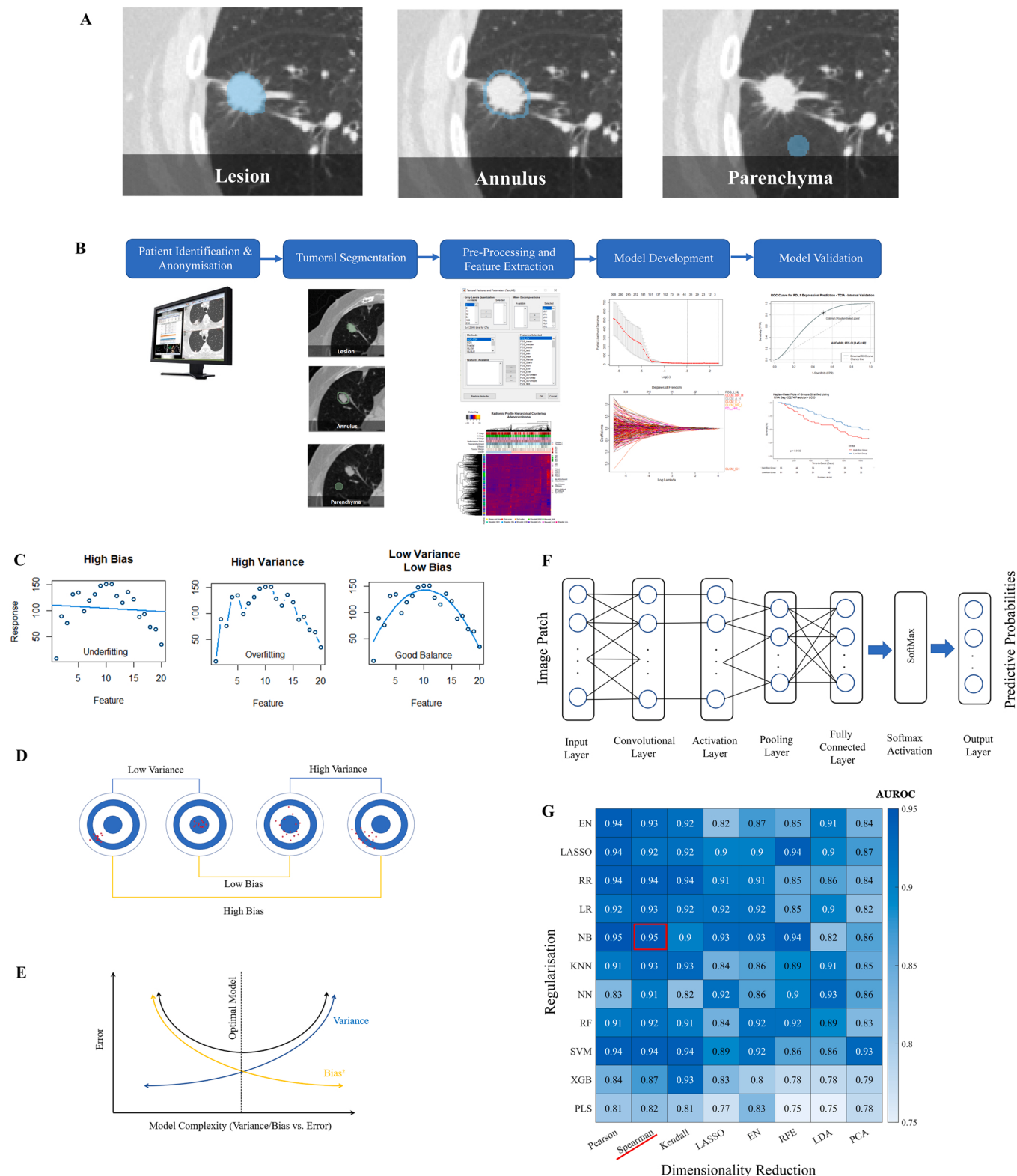


Fig. 3. Radiomics workflow. A. Segmentation methodology in multi-regional radiomics. B. Standard radiomics extraction and model development workflow. C. The effects of bias and variance on model fitting. D. Illustrations of bias and variance on data spread (red points) and fitted models. E. The plots of error against model complexity for bias and variance to illustrate importance of balancing these characteristics when developing a model with optimal complexity. F. Deep learning-based model architecture. G. Heatmap showing statistical learning-based model development. The combination of dimensionality reduction and regularisation methods giving the highest AUROC is outlined in red. EN: Elastic Net, RR: Ridge Regression, LR: Logistic Regression, NB: Naïve Bayes, KNN:K-Nearest Neighbours, NN: Neural Net, RF: Random Forest, SVM: Support Vector Machine, XGB: eXtreme Gradient Boost, PLS: Partial Least Squares; RFE: Recursive Feature Elimination, LDA: Linear Discriminant Analysis, PCA: Principal Component Analysis.

Table 2
Common machine learning methods used in radiomics model development.

Method	Model/Algorithm Highlight	Description
Linear Regression	$y = \beta_0 + \sum_{i=1}^n \beta_i x_i$	Generic/numeric outcome modelling
Logistic Regression	$y = \frac{1}{1 + \exp(-\beta_0 + \beta_1 x)}$	Binary outcome modelling
Cox Regression	$y(t) = y(0)\exp(\sum_{i=1}^n \beta_i x_i)$	Survival outcome modelling
Least Absolute Shrinkage and Selection Operation (LASSO)	$\hat{\beta} = \operatorname{argmin}_{\beta} (\ y - X\beta\ ^2 + \lambda \ \beta\ _1)$	Includes regularisation which introduces some model bias to reduce variance
Ridge Regression	$\hat{\beta} = \operatorname{argmin}_{\beta} (\ y - X\beta\ ^2 + \lambda \ \beta\ _2^2)$	Similar to LASSO, with better shrinkage but more complex models
Elastic Net Regression	$\hat{\beta} = \operatorname{argmin}_{\beta} (\ y - X\beta\ ^2 + \lambda_1 \ \beta\ _1 + \lambda_2 \ \beta\ _2^2)$	Combines the penalty terms of LASSO and ridge regression for balanced performance
Recursive Feature Elimination (RFE)	for i in $[1 : p]$: model training with feature set $\hat{x}_i \quad \hat{x}_{i+1} = \hat{x}_i$ - last ranked feature x_i	Iterative feature removal and model training
Naïve Bayes (NB)	$y = \operatorname{argmax}_y P(y) \prod_{i=1}^n P(x_i y)$	Bayesian probabilistic estimates
Random Forest (RF)	$y = \sum_{u=1}^C f_i(1 - f_i)$	Decision tree ensembles with bootstrap aggregation
Support Vector Machine (SVM)	$y_i(w \cdot x_i + b) - 1 \geq 0 \quad \text{for } y_i = +1, -1$	Hyperplane separation with kernel trick transformation
K-Nearest Neighbours (KNN)	$P(y=j X=x) = \frac{1}{K} \sum_{i \in A} I(y^i = j)$	Minimising the spatial distance to datapoints
Principal Component Analysis (PCA)	$T_L = XW_L$	Eigen decomposition of feature space T_L into eigenvectors, or components, W_L
K-Means Clustering	$\operatorname{argmin}_{c_i \in C} \operatorname{dist}(c_i, x)^2$	Assigns datapoints x to clusters based on their geometric distance $\operatorname{dist}(c_i, x)^2$ to their centroid c_i
Convolutional Neural Network (CNN)	$G[m, n] = (f^* h)[m, n] = \sum_j \sum_k h[j, k] f[m - j, n - k]$	Multi-layered deep learning network

datasets with known response outcomes (“labelled data”) and are examples of supervised learning. Principal component analysis (PCA) offers an unsupervised framework where significant features are determined based on eigen decomposition of the feature space [60]. It was found to be less prone to overfitting than supervised models, due to the inclusion of feature interaction effects that are missing from many supervised methods [61]. K-means clustering is yet another unsupervised method, that performs data separation based on their geometric distance to cluster centroids [62].

Sometimes, a wrapper framework can be used, such as recursive feature elimination (RFE) combined with SVM, where a dynamic group of features are tested with the least significant feature excluded after each iteration, to improve feature selection accuracy [63].

The error term of model estimate $f(x)$ for an actual value $f(x)$ can be written as Eq. (4):

$$\begin{aligned} Err(x) &= E[(f(x) - \hat{f}(x))^2] = (E[\hat{f}(x)] - f(x))^2 + E[(\hat{f}(x) - E[\hat{f}(x)])^2] + \sigma^2 \\ &= \text{Bias}^2 + \text{Variance} + \text{Irreducible Error} \end{aligned} \quad (4)$$

where $E(f(x))$ is the true expectation of $f(x)$ and σ^2 the irreducible error, which are plotted against error and model complexity in Fig. 3C-E. The optimal model would be one that balances bias and variance. Conventional methods such as linear regression driven by ordinary least squares

suffer from underfitting due to their high bias. Non-parametric methods such as RF and KNN, on the other hand, are more susceptible to overfitting. Ridge, least absolute shrinkage and selection operation (LASSO), and elastic net regressions are a group of supervised methods that include regularisation penalty terms to reduce model complexity, and thereby achieving a desirable trade-off between model bias and variance [64]. In ridge regression, the loss function becomes Eq. (5):

$$\sum_{i=1}^n \left(y_i - \sum_{j=1}^p x_{ij} \beta_j \right)^2 + \lambda \sum_{j=1}^p \beta_j^2 \quad (5)$$

where $\lambda \sum_{j=1}^p \beta_j^2$ is the *L2 norm* penalty that shrinks the regression coefficients with minor contribution to the outcome. In LASSO, an *L1 norm* term, $\lambda \sum_{j=1}^p |\beta_j|$, is used instead, which removes the less significant coefficients instead of merely shrinking them. This has the advantage of creating less complex models when the outcome is heavily influenced by a few features in a large feature space. Incorporating the strengths of both methods, elastic net regression includes both penalty terms with adjustable weights. For these advantages, LASSO and elastic net regression are commonly used in the latest lung cancer radiomics models [65–67].

Deep learning methods based on convolutional neural network (CNN) (Fig. 3F) are being explored as an alternative to hand-crafted radiomics [53,68–72]. In this framework, features are not pre-defined, and accurate tumour segmentations are no longer essential, which confer notable advantages because the latter is a major source of feature inaccuracy and variability in conventional radiomics [69]. A fixed size cropped image patch/volume containing the tumour is fed into a multi-layer network, which is constructed based on millions of parameters estimated through training and parameter tuning. Through convolution and pooling of data, the input image is encoded into data representations, from which deep learning features are extracted. These are converted into a unidimensional array, that is ultimately passed onto a fully connected layer to give final predictive probabilities for each outcome label. The network can be constructed *de novo* or based on a pre-existing one trained on natural images with parameters updated via transfer learning; the latter is more widely adopted in current literature due to training sample sizes. Comparable performance to hand-crafted radiomics has been demonstrated in a small study without external validation for time-to-event outcome prediction in lung cancer [69]. Despite its stated advantages, deep learning-based model development can be hindered by small training sample size, and model utility affected by poor interpretability. One solution to the latter is activation mapping, where the final convolutional layer is used to generate a heatmap to highlight regions having the most influence on model predictions, which are then radiologically interpreted for meaning [72].

Model training strategy remains an area under active research. Algorithm benchmarking, such as the one shown in Fig. 3G for hand-crafted features, can be undertaken, particularly when dealing with new clinical or histopathological outcomes for prediction, where there is less prior knowledge.

2.6. Model validation

Arguably the most crucial part of the radiomics pipeline is testing the developed model with external independent data. The rationale is to control for model overfitting; and ascertain the model’s robustness or generalisability when applied to data other than that of the discovery cohort. As discussed earlier and illustrated in Fig. 3C-E, the ideal model would be one with an optimal trade-off between bias and variance, which not only captures the patterns in its training data but also generalises well in testing data.

External data are acquired in a different institution, and preferably on varied scanner and acquisition parameter settings. Public domain data are often used, such as NSCLC Radiogenomics, Clinical Proteomic

Tumor Analysis Consortium squamous cell carcinoma (CPTAC-LSCC), adenocarcinoma (CPTAC-LUAD), and the Cancer Genome Atlas Program squamous cell carcinoma (TCGA-LUSC), and adenocarcinoma (TCGA-LUAD) datasets, for NSCLC [73–75]. The preference is to involve more than one external testing dataset, though this may not always be feasible.

For binary or categorical outcomes such as treatment response, the model's predictive performance can be quantified as area under the receiving operating curve (AUROC) or F1 score. For prognostication, Cox proportional hazards ratio and log-rank test p-value are normally used. A model's reported performance should be assessed in a clinical

and practical context. For example, for patient prognostication, the model's performance could be benchmarked to that using tumour volumetry, performance status, and/or tumour staging; and for PD-L1 inhibitor immunotherapy response prediction, compared to that predicted using PD-L1 expression on IHC, in both cases mirroring the current clinical practice.

2.7. Multi-omics analysis

Clinical features such as age, gender, performance status, prior cancer treatment, family, smoking and alcohol history have been used

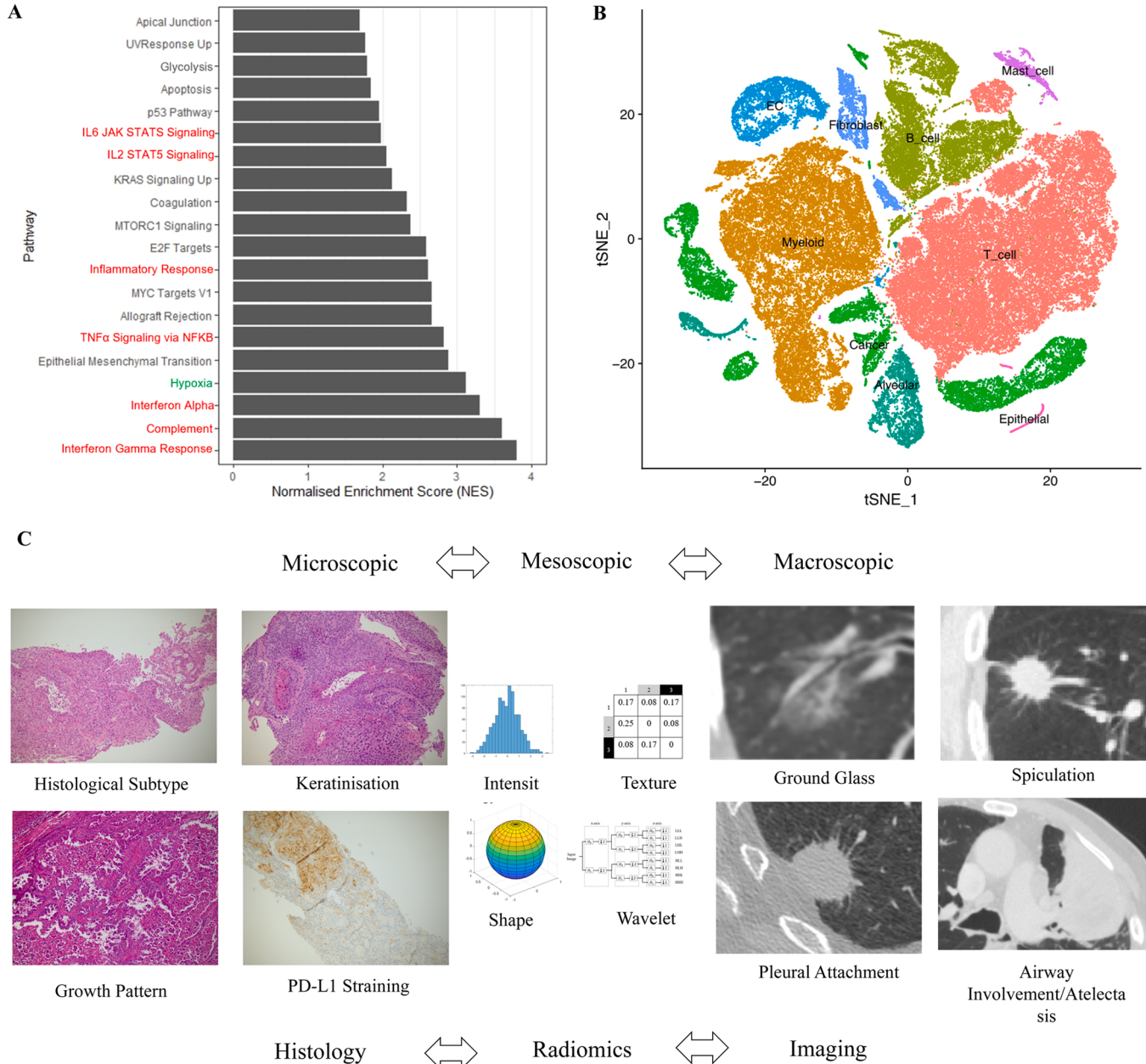


Fig. 4. Genomic and transcriptomic correlates of radiomic features in a predictive model. A. Gene set enrichment analysis of a predictive model for CD274 (protein encoding gene for PD-L1). Shown in the figure are ten pathways with highest correlations. Note most pathways are either inflammation (red) or hypoxia (green)-related, which is consistent with the immunobiological understanding that a responding tumour tends to demonstrate sustained immune response through upregulated inflammation. B. Single cell RNA sequencing analysis t-distributed stochastic neighbour embedding (t-SNE) plots showing that T-cell and myeloid cell populations are most highly expressed in the most correlated genes. C. Schematics showing radiomics as mesoscopic features that bridge the imaging and histological feature spaces. The histological slides on the left show (in clockwise order from the top left): AdC with different histological subtypes, SCC with evidence of keratinisation, intratumoral variation of PD-L1 staining, and high magnification view of lepidic and papillary growth patterns in AdC. The CT images on the right show (in clockwise order from the top left): Pure ground glass AdC, margin spiculation, marked airway involvement with distal lung collapse, and pleural attachment.

for developing prognostic models in lung cancer [76]. In radiomic works, they have been used to construct comparison models to benchmark the performance of radiomics-based models, or combined with radiomics features using multivariable regression, or nomogram, to enhance model performance [77,78].

Advancements in genomic sequencing technology, such as RNA microarray and quantitative reverse transcriptase polymerase chain reaction (qRT-PCR), have paved way for the development of genomics-based models for patient prognostication and treatment response prediction in lung cancer [79]. Several studies have presented genomics-based models for early-stage NSCLC, with effective prognostic stratification of patients into high and low risk groups, superior to the performance of TNM staging [79–81]. The key limitation of genomics-based methods is their dependence on tissue sampling, which is invasive and susceptible to issues arising from tumour heterogeneity and evolving mutations. With the emergence of driver mutation targeting therapy, next generation sequencing has now become the standard of care in selected patient groups. Like clinical features, where available, genomics can be integrated with radiomics in a multivariable framework for improved performance.

Radiogenomics combines radiomics with genomic phenotypes to

develop models predictive of patient outcomes [82]. This field has attracted much interest in recent years for its role in guiding personalised treatments [83,84]. In these studies, radiomic features have been developed to predict for target driver mutations, such as epidermal growth factor receptor (EGFR) and anaplastic lymphoma kinase (ALK) mutations.

Models aimed at guiding PD-1/PD-L1 immunotherapy can be developed to predict for CD8 [85,86] or CD274 gene expression, the latter being the protein encoding gene for PD-L1 [66]. These models might be superior to one directly developed for PD-L1 expression, because the latter would be susceptible to variabilities pertaining to staining technique [87] or partial sampling of a histologically heterogeneous tumour [88,89].

To advance the understanding of the disease process and treatment, radiomics models can be further analysed for their biological correlates using genomic and transcriptomic methods. By integrating radiomics with transcriptomics using gene set enrichment analysis (GSEA), the most significantly correlated cellular pathways with the model's component features are established (Fig. 4A). Further integration of the correlated cellular pathways with single cell RNA sequencing (scRNA-seq) data can allow the cell populations expressing the most correlated

Table 3
Summary of reviewed literature on radiomics-based lung cancer virtual biopsy.

Reference	Prediction Target (s)	Model Features ^a	Training Cohort	Mode of Validation	Validation Cohort ^b	Best Performance ^c
Wu et al. [58]	Histology subtype	Radiomics features	N = 198	External	n = 152	0.72
Ferreira Junior et al. [77]	Histology subtype	Clinical and radiomics features	N = 52	Internal	N = 16	0.81 (Subtype) 0.75 (Nodal involvement) 0.71 (Distant metastasis)
Qi et al. [90]	Nodal involvement					
	Distant metastasis					
Chen et al. [91]	Histological subtype	CT radiomics	N = 321	Internal	N = 96	0.87 (SCLC) 0.84 (AdC) 0.76 (SCC)
Perez-Johnston et al. [92]	Micropapillary or solid growth pattern	CT radiomics and semantic features	N = 103	Internal	N = 55	0.86 (micropapillary or solid growth pattern)
Chen et al. [93]	For growth patterns, lymphovascular invasion, Bronchogenic growth; various driver mutations; Risk of recurrence	CT radiomics	N = 219	N/A ^d	N/A	Clusters with enrichment of the studied clinical and histological features.
Xu et al. [94]	Bone metastases	Resected AdC				
	Post-treatment brain metastasis	CT radiomics	N = 137	Internal	N = 58	0.73
Cheng et al. [100]	ALK positive AdC					
Li et al. [96]	EGFR 19Del and L858R	CT radiomics	N = 106	External	N = 26	0.682
Yang et al. [102]	EGFR mutation	CT radiomics	N = 464			0.803
Hao et al. [78]	EGFR 19Del and L858R					
	T790M mutation	CT radiomics	N = 236	Internal	N = 76	0.79 (19Del) 0.78 (L858R)
Chang et al. [103]	ALK rearrangement	CT radiomic, clinical and CT semantic features	N = 186	Internal	N = 74	0.71
Tian et al. [104]	ALK rearrangement	PET-CT radiomic features	N = 154	Internal	N = 39	0.914
Wang et al. [107]	PD-L1 positivity ($\geq 50\%$)	CT radiomics	N = 367	Internal	N = 159	0.88
Sun et al. [86]	PD-L1 expression	CT radiomics	N = 750	External	N = 96	0.76
	CD8 gene expression					
	Tumour immune phenotype					
Shao et al. [109]	CD8 gene expression	CT radiomics	N = 135	External	N = 119 (CD8 gene expression)	0.67 (CD8 gene expression)
	Tumour immune phenotype		Several tumour types, of which 30 were of the lung		N = 100 (tumour immune phenotype)	0.76 (tumour immune phenotype)
	10-panel predictions (various driver mutations & PD-L1 positivity - $\geq 50\%$)	CT radiomics	N = 876	Internal	N = 110	0.950 (< 1%) 0.934 (1–49%) 0.946 ($\geq 50\%$)
						0.796 (EGFR) 0.867 (ALK) 0.680 (BRAF) 0.816 (KRAS) 0.912 (PD-L1 positivity)

^aBest performing model

^bExternal validation where available otherwise internal.

^cBest AUROC from external validation where possible, otherwise internal. Non-AUROC findings are as stated.

^dCluster analysis only. No AUROC assessed.

genes to be identified (Fig. 4B). This knowledge could help confirming or refuting conceptual hypotheses about the role certain cell populations or pathways play in an effective treatment.

3. Precision medicine for lung cancer

3.1. Overview

The main applications of radiomics for lung cancer treatment are virtual biopsy and clinical outcome prediction. Virtual biopsy addresses the issues of intra-tumoral heterogeneity, evolving mutations, and inadequate sampling, by non-invasively predicting for tumour histology and driver mutations to aid in therapeutic planning. In clinical outcome prediction, patient prognosis, treatment response, disease recurrence or progression, and treatment side effects are predicted, for patients undergoing treatment options including SABR, radical radiotherapy, chemotherapy, targeted therapy, and immunotherapy. The reviewed

literature in this section are summarised in Tables 3 and 4.

3.2. Virtual biopsy

3.2.1. Tumour histology

Models based on handcrafted radiomic features (first order statistics and higher order wavelet-decomposed features) have been shown to be predictive of tumour histological subtype (SCC or AdC) in NSCLC, achieving AUROCs of 0.72 [58], and 0.81, respectively [77]. The integration of clinical data did not improve model performance in the latter study [77]. A deep learning model has achieved a one-stop histological classifier for lung cancer, where NSCLC, as well as SCLC histologies were predicted, to an accuracy of AUROC = 0.87 (SCLC), 0.84 (AdC) and 0.76 (SCC) [90].

In AdC, micropapillary and solid growth patterns are high grade histological features associated with worse prognoses and often require more radical surgical resection and adjuvant chemotherapy. Radiomics

Table 4

Summary of reviewed literature on radiomics or deep learning feature-based clinical outcome prediction for lung cancer.

Reference	Prediction Target (s)	Model Features ^a	Training Cohort	Mode of Validation	Validation Cohort ^b	Best Performance ^c
Sepehri et al. [59]	3-year overall survival	PET-CT radiomics	N = 87	Internal	N = 51	0.78
Chen et al. [110]	3-year overall survival	CT radiomics	N = 145	External	N = 65	0.67
Arshad et al. [50]	14-month overall survival	PET-CT radiomics	N = 133	External	N = 21	Risk stratification achieved (log-rank p < 0.05)
Afshar et al. [69]	Time to event	PET-CT deep learning features	N = 106	Internal	N = 26	Risk stratification achieved (p < 0.05)
Kim et al. [116]	5-year disease-free survival	CT radiomics, genomics and clinical features	N = 124	Internal	Unknown	0.79 (clinical only) 0.84 (clinical & genomics) 0.86 (clinical & radiomics) 0.87 (all three)
Hosny et al. [72]	2-year overall survival post-radiotherapy and post-surgery	CT deep learning features	N = 293 (radiotherapy) N = 183 (surgery)	External	N = 211 (radiotherapy) N = 97 (surgery)	0.70 (radiotherapy) 0.71 (surgery)
Lafata et al. [117]	Tumour recurrence after SBRT	CT radiomics	N = 56	Internal	N = 14	Two features identified to be associated with post-treatment recurrence
Dissaix et al. ¹¹⁸	Disease recurrence after SBRT	PET-CT radiomics	N = 64	External	N = 23	0.91
Hindocha et al. [112]	Disease recurrence after radical radiotherapy; 2-year RFS	CT radiomics and clinical features	N = 302	External	N = 132	0.738 (recurrence) 0.755 (RFS)
Lou et al. [71]	Treatment failure post-SBRT	CT deep learning features	N = 849	Interval	N = 95	Risk stratification achieved (p < 0.05)
Chang et al. [119]	Chemotherapy response	CT radiomics	N = 272	External	N = 43	0.85
Wei et al. [120]	Chemotherapy response in SCLC	CT radiomics	N = 92 ^d	Internal	Not given	0.797
Yang et al. [121]	Response to EGFR-TKI	CT radiomics	N = 253	Internal	Unknown ^e	0.90
Trebeschi et al. [122]	Response to or stability following PD-1 inhibition immunotherapy	CT radiomics	N = 123	External	N = 262	0.79
Moran et al. [123]	Early lung injury changes	CT radiomics (GLCM features)	N = 14 (48 baseline and follow-up scans)	Internal	N/A	0.75
Huang et al. [124]	Radiation pneumonitis post-SBRT	Dosimetric features and deep learning features	N = 112	Internal	N = 28	0.90
Mattonen et al. [125]	Distinction of disease recurrence from benign post-radiation changes	CT radiomics	N = 45 (182 baseline and follow-up scans)	Internal	N/A ^f	0.85
Chen et al. [66]	Response to PD-1/PD-L1 CBI Pneumonitis occurrence	CT radiomics	N = 85	External	N = 109	0.68 (treatment response) 0.66 (pneumonitis occurrence)

^aBest performing model

^bExternal validation where available, otherwise internal.

^cBest AUROC from external validation where possible, otherwise internal. Non-AUROC findings are as stated.

^dTotal study size: 92.

^eTotal study cohort size: 253. No information available on the internal validation cohort size.

^fBenchmarked to human observers

have been shown to be predictive of such patterns in early stage AdC in both a composite vector (*GLCM texture variance* and *75th percentile intensity* features, AUROC of 0.86) [91] and unsupervised clustering paradigm [92].

3.2.2. Tumour staging

Radiomics has also demonstrated a potential role in tumour staging, by predicting for nodal involvement and distant metastasis. An AUROC of 0.84 has been achieved in one study for nodal involvement prediction, using only radiomics features [77]. This improved to an AUROC of 0.87, when clinical (age, sex, smoking status, other known tumour) and radiological features (lobar location and diameter of the tumour) were incorporated. In another work [93], bone metastases from NSCLC were found to be significantly associated with texture feature *glszm_Small Area High Gray Level Emphasis* (OR = 0.016, 95% CI: 0.001–0.286, $P = 0.005$), which has the most significant odds ratio in a multivariable composite model that also included patient's sex, Cyfra-21, serum iron level, and lesional homogeneity and pleural indentation sign on CT. Brain metastases, in a separate work, were found to be associated with wavelet-texture feature *W_GLCM_LH_correlation* [94].

3.2.3. Tumour genotype

In NSCLC, common driver mutations include EGFR (10–30%), fibroblast growth factor receptor 1 (FGFR1; 20%), Kirsten rat sarcoma viral oncogene (KRAS; 15–30%), phosphatidylinositol-4,5-bisphosphate 3-kinase, catalytic subunit alpha (PIK3CA; 2–5%), human epidermal growth factor receptor 2 (HER2, 2–5%), v-RAF murine sarcoma viral homolog B1 (BRAF), and ALK (3%), with the numbers in brackets indicating their respective prevalence [95].

Of these, EGFR is the most commonly targeted mutation [96–99]. The latest CT radiomics-based model for EGFR mutation prediction has achieved an AUROC of 0.80 in external validation [100]. Given the differences in survival and treatment strategy in patients with the two main subtypes of EGFR mutations [62], namely 19Del (exon 19) and L858R (exon 21), radiomics have been able to distinctly predict these subtypes, to a reasonable degree of success (AUROC of 0.79 and 0.78, for 19Del and L858R, respectively) [96,101]. T790M (exon 20) mutation is an acquired mutation that patients receiving first- or second-generation EGFR tyrosine kinase inhibitor (TKI) can develop after 9–12 months of treatment, which is believed to be associated with drug resistance in these patients [102]. Predictors for T790M have been developed based on CT-derived radiomics, achieving an AUROC of 0.76 [102].

ALK rearrangement mutation is another treatment target. Prediction is feasible using CT radiomics, achieving an AUROC of 0.914 when combined with clinical and CT semantic features [78]. This performance was better than that based on clinical (0.735) or radiomic features alone (0.890) [78]. PET-CT radiomics model showed a performance of AUROC 0.88, which was not improved with clinical features incorporation [103]. Neither work was externally validated.

Radiomics-based prediction of PD-L1 positivity has achieved an AUROC of 0.76 for PD-L1 $\geq 50\%$ [104]. However, due to the lack of consensus on the PD-L1 expression cut-off for treatment, lower thresholds are typically used in clinical practice (such as $\geq 1\%$) [105,106]. In a separate study, a CT-radiomics model predictive of the different levels of PD-L1 has been developed, achieving AUROC of 0.950, 0.934 and 0.946 for PD-L1 $< 1\%$, 1–49% and $\geq 50\%$, respectively [107].

Because PD-L1 expression is a dynamic and variable quantity, adopting a positivity threshold is thought to be overly simplistic [108]; and is susceptible to data variability depending on the IHC assay used [108]. Therefore, there is a growing interest in using genomic correlates as the response vector for developing models for PD-1/PD-L1 inhibition immunotherapy. A model developed based on CD8 gene expression was found to be predictive of CD8 infiltration (AUROC 0.67) in a mixed cohort of patients (including NSCLC) treated with PD-1/PD-L1 inhibitor immunotherapy, as well as their response to treatment [86].

To reflect the realistic clinical scenario where a large panel of driver

mutations and PD-L1 would be evaluated by molecular and IHC testing, efforts have been made on developing multivariate models for simultaneously predicting various driver mutations. One such model has achieved reported an AUROC of 0.796, 0.867 and 0.912, for EGFR, ALK and PD-L1 positivity ($\geq 50\%$) respectively [109].

3.3. Clinical outcome prediction

3.3.1. Prognostication

Patient prognostication or survival prediction is amongst earliest applications of lung cancer radiomics [28]. This can either be achieved using CT radiomics, such as one achieving an AUROC of 0.67 for 3-year overall survival (OS) in an external validation dataset of mixed NSCLC cases [110], or PET-CT radiomics, where statistically significant stratification of patients into high and low risk survival groups has been achieved with hand-crafted radiomics [50], and deep learning features [69].

Furthermore, the use of radiomics for the prognostication of NSCLC patients receiving specific treatments has also been extensively studied and reported [111–115]. Deep learning features have also shown reasonable performance in both post-radiotherapy (AUROC 0.70) and post-surgical (AUROC 0.71) cohorts [72].

In a separate prognostic study, integrating clinical and genomic features was found to improve model performance from AUROC 0.79 (clinical features only) to 0.86 (clinical and radiomic features) and 0.87 (clinical, genomic and radiomic features) [116].

3.3.2. Treatment response and disease recurrence

In SBRT-treated NSCLC, two radiomic features have been identified to be associated with local failure, namely, *homogeneity* and *long-run-high-gray-level-emphasis* [117]. Similarly, two PET-CT radiomic features, *PET IC2* and *CT flatness*, have been noted for their associations with tumour recurrence post-SBRT, and shown to be predictive of the latter in external validation with an AUROC of 0.905 [118]. CT deep learning features were shown to be predictive of treatment failure in SBRT, and a proposed role for guiding dose reduction [71].

For those receiving radical radiotherapy, CT-based radiomics (particularly *GLSZM zone percentage*) can predict disease recurrence within 2 years following treatment to an AUROC of 0.673, which further improves to 0.738 once clinical features such as age, performance status, body mass index, smoking status and tumour stage are incorporated [112].

For chemotherapy response prediction for NSCLC, an AUROC of 0.85 was reported in the external validation of a CT radiomics model [119]. For response prediction for chemotherapy-treated SCLC, an AUROC of 0.797 was reported, which was better than one using known clinical features including tumour stage (AUROC = 0.670) [120].

Regarding targeted therapy, for EGFR-tyrosine kinase inhibitor (TKI)-treated NSCLC, CT radiomics predicted the response to an AUROC of 0.90, [121] while for NSCLC treated with PD-1/PD-L1 CBI, a recent CT-radiomics model has achieved an AUROC of 0.79 for predicting non-disease progression [122]. Another model developed based on CD274 count reported an AUROC of 0.68 for predicting treatment response in this patient group [66].

3.3.3. Adverse events

Radiation-induced lung injury changes on CT following SBRT are detectable with radiomics, which correlates also with dose and fractionation. [123] Most recently, a larger study ($n = 140$) has shown the possibility of using a combination of CT dosimetric and deep learning (ResNet) features to improve this prediction, up to an AUROC of 0.90 [124].

Radiomics can also distinguish post-treatment recurrence from radiation-related lung changes on follow-up CT, achieving an AUROC of 0.85 [125].

Pneumonitis occurrence in patients treated with PD-1/PD-L1 CBI has

been predicted to an AUROC of 0.66 [66].

4. Discussion and future prospects

Over the last five decades, even with newer treatments and disease screening, the long-term survival rate of lung cancer has not improved substantially compared to in other malignancies [126]. This can be attributed to disease complexity: despite the prevalence and significant health challenge of lung cancer, our knowledge about the geospatial architecture of its cell populations and mode of evolution remains limited [27]. The histological heterogeneity of lung cancer is due to the presence of multiple cell subpopulations, with varying tendencies to grow, invade, or metastasise [127]. Whole-exome sequencing has revealed treated metastases to harbour new driver mutations not found in untreated metastases [128]. This *de novo* mutation is believed to be the source of acquired treatment resistance.

Radiomics offers a new high-throughput approach to interpreting imaging data. It has the remarkable ability to capture *mesoscopic* tumoral features that are present in the imaging data but not readily observable to human eye [65,129]. This bridges imaging ('macroscopic') with histology ('microscopic') and unfolds a new dimension for assessing cancer structure. (Fig. 4C) In one study, texture-feature *GLCM inverse difference* was found to be the most representative feature (an *avatar feature*) in a model predictive of poor outcome in patients treated with CBI [130]. This feature is positively correlated with *CAIX expression*, a key enzyme upregulated in tumour hypoxia, and associated with an acidic TME [130]. Given the role of hypoxia in tumoral progression, angiogenesis, and the development of treatment resistance [131], the finding would suggest a conceptual framework expounding the interplay of these biological processes within the TME, and as the basis for promoting rapid tumoral progression and stalling treatment response in these patients.

Prior reports on PET imaging and radiomics have inspired new thoughts on lung cancer evolution. The shift of voxel of maximal metabolic activity from the centre of the tumour is found to be associated with a worse prognosis in NSCLC [132]. The distribution of metabolic activity shows increasingly metabolically active proliferative cellular spots from the tumoral centre to the periphery, postulated to demonstrate competitions between tumoral cell subpopulations, with more aggressive phenotypes sited more peripherally. On PET radiomics, *GLSZM_SzVarianc_64gl* and *NGTDM_Complex_64gl_FVX* were found to be associated with worse patient prognoses, both of which are indirect measures of tumour heterogeneity and therefore their high values can be a manifestation of cancer cell population diversity [50].

Newer treatments for lung cancer include targeted therapy and immunotherapy, which target specific driver mutations and transmembrane receptors, respectively. Their efficacy is therefore closely related to the identification of such biomarkers for selecting suitable treatment candidates. Conventional practice achieves this by focal tissue sampling followed by IHC or molecular tests, which only examines a fraction of the tumour at one point in time; and is therefore limited by the pronounced intra-tumoral heterogeneity and evolving mutations in lung cancer. Radiomics can overcome these limitations by assessing the whole tumour, including the peritumoral region in multi-region radiomics, and at any time when suitable imaging is acquired, in addition to being non-invasive and low-cost. The high throughput nature of radiomic features enables the deployment of advanced machine learning methods to expedite workflow.

Comparing to models developed based on clinical features, radiomics-based models always showed superior performance on the same testing data [78,116]. Some radiomics models have been compared to the ones integrated with clinical, genomic, or radiological semantic features, sometimes with improved performance [77,78,91, 112,116]. It's important not to overlook the importance of these features for model optimisation. However, the inclusion of these additional features should be undertaken with care, because of the potential

interactions between features from different groups and confounding effects with certain clinical outcomes. For example, when predicting for treatment response in patients treated with EGFR-targeting TKI, EGFR mutation status should not be included in model training, as it would invariably be positive and diminish the influence of other key features on the predictive signature.

Whilst there is an abundance of literature on NSCLC, the application of radiomics to SCLC remains scarce. Other than SCLC histology [90] and chemotherapy response predictions [120], there is little work on SCLC radiomics which is likely due to a combination of limited available treatment options, and segmentation difficulty, as many SCLC are centrally located when diagnosed and tend to have contiguous nodal and/or mediastinal masses.

4.1. Challenges to radiomics for lung cancer treatment

Despite its well-established potential for advancing precision cancer treatment, lung cancer radiomics is constrained by several key burdens. First, its research appeal has generated a large amount of literature in recent years, many of which are lacking in standardised methodology and reporting. One review assessed NSCLC radiomics papers up to 2019 and found a very low mean RQS score of only 2.5 out of 36 [133]. Arguably, the area most in need of attention is external validation, with even the latest published models often lacking validation with an independent test set. This inadequacy can be addressed using the ever-expanding collection of publicly available imaging datasets such as those on the Cancer Imaging Archive (TCIA), which are often paired with clinical, histological, and genomic/transcriptomic data. On a related note, models predicting for outcomes in a more specific patient group, such as those for adverse events in CBI, can be often limited by the small sample size available, both locally and in the public domain. This limitation unfortunately is more difficult to overcome so should be carefully considered when designing a study, to give enough statistical power and on selecting the best model development strategy.

Finally, feature consistency and reproducibility should be ascertained by maximising the adherence to IBSI, which is being constantly reviewed for its list of recommended features [21]. All studies should be reported in accordance to the TRIPOD guidelines to deliver the best comparability and replicability [36].

Deep learning offers an alternative to conventional hand-crafted radiomics. It alleviates the model's dependence on an accurate tumour segmentation and feature definition, thus improves feature consistency and reproducibility, and reduces the workload required for data curation. However, its adoption in the current literature remains limited, which might be due to its large training dataset requirement and sub-optimal model interpretability.

4.2. Future prospects

Lung cancer radiomics offers abundant further research opportunities.

SBRT is associated with a synergistic effect with subsequent immunotherapy, which might be related to the potentiation of inflammatory cellular pathways [134]. A radiomics-model developed for *CD8* gene expression for a mixed cancer cohort treated with SBRT and PD-1/PD-L1 inhibition immunotherapy has reported an AUROC of 0.63 for response prediction [85]. This paves way for a dedicated model for this treatment scenario, which can potentially also give insight into the exact cellular mechanism underpinning the synergy, by integrating genomic and transcriptomic data using methods illustrated in Fig. 4A and B.

Whilst many driver mutations have been discovered in NSCLC, only a handful are currently treatment targets. As newer mutation targeting agents emerge, such as those targeting neurotrophic tropomyosin-related kinases (NTRK) fusion mutation [135], there is scope for developing their radiomics-based predictive models. Likewise, in CBI, cytotoxic T lymphocyte antigen 4 (CTLA4) is expressed in some cases

and with routine use of dual CTLA4-PD-L1 immunotherapy [136], radiomics might be explored for its role in guiding such treatment and for predicting clinical outcomes in such situation.

Lung metastases evaluation is another emerging topic for radiomics. In an earlier study, CT radiomics were shown to be able to discriminate lung metastases from solitary primary lung tumours, with an AUROC of 0.92 [137]. With preliminary results showing the utility of radiomics in predicting clinical outcomes in lung metastases from melanoma primary treated with CBI [86], it's a promising field warranting further investigation [86].

Liquid biopsies are minimally invasive methods that use serum biomarkers to facilitate precision medicine. Prior studies have explored combining them with radiomics to improve on their performance [95]. In one such work, plasma-derived cell free DNA (cfDNA) analysed by digital droplet polymerase chain reaction (ddPCR) test was integrated with radiomic features for EGFR mutation prediction [138]. Given the minimally invasive nature of both methods, liquid biopsy and radiomics can be both acquired and used alongside each other once their complementary and synergistic utilities are established.

Delta radiomics is a newer concept that targets the variation in features resulting from a documented change in the disease or its management, such as the commencement of a treatment or the confirmation of a second mutation. Delta radiomics in patients treated with radiotherapy have been found to be associated with worse prognoses [139]. There are currently limited publications in this domain, with preliminary results suggesting a potential role for delta radiomics in EGFR mutation prediction, and prognostication in chemoradiation therapy and CBI [140].

The issues of limited sample size and external validation can be addressed by federated learning, that is, using a data privacy preserving framework to facilitate multi-centre collaboration. In this decentralised setup, model training takes place locally, minimising the risk of data privacy breach. The trained model parameters are then securely aggregated onto a central server to update the baseline models. For handcrafted radiomic features, one such framework has been proposed for head and neck cancer radiomics [141], which might be adopted and tested for lung cancer use. A more secure framework is offered by swarm learning, where the models are amalgamated via a secure network in the absence of a central server. This advanced setup has seen pilot use in chest x-ray interpretation but has not yet been implemented in radiomics-related applications [142].

For its stated advantages, deep learning will continue to be an active research area as available datasets expand, through multi-centre collaborations aided by federated learning [70].

Funding Source

This work was supported with funding from the Imperial College Biomedical Research Centre award (WSSC P87324, P62585). Additionally, MC is supported by the Academy of Medical Sciences award SGL026\1024, and PV is supported by Imperial College Healthcare NHS Trust BRC. The study funders did not have a role in the design and conduct of the review, opinions expressed; or the decision to submit for publication.

CRediT authorship contribution statement

Mitchell Chen: Conceptualization, Methodology, Formal analysis, Investigation, Writing – original draft, Writing – review & editing, Visualization, Project administration. **Susan J. Copley:** Conceptualization, Resources, Writing – review & editing, Project administration, Funding acquisition. **Patrizia Viola:** Resources, Visualization, Writing – review & editing. **Haonan Lu:** Formal analysis, Visualization. **Eric O. Aboagye:** Conceptualization, Resources, Writing – review & editing, Project administration, Funding acquisition.

Declaration of Competing Interest

HL received consulting fees from BerGenBio, and grants from Air Theranostics Ltd. All other authors declare no conflicts of interest.

Data availability

No data was used for the research described in the article.

References

- [1] H. Sung, J. Ferlay, R.L. Siegel, et al., Global Cancer Statistics 2020: GLOBOCAN estimates of incidence and mortality worldwide for 36 cancers in 185 countries, CA Cancer J. Clin. 71 (3) (2021) 209–249, <https://doi.org/10.3322/caac.21660>.
- [2] X. Yin, H. Liao, H. Yun, et al., Artificial intelligence-based prediction of clinical outcome in immunotherapy and targeted therapy of lung cancer, Semin Cancer Biol. 86 (2022) 146–159, <https://doi.org/10.1016/J.SEMCANCER.2022.08.002>.
- [3] A. Jemal, R. Siegel, E. Ward, et al., Cancer statistics, 2008, CA Cancer J. Clin. 58 (2) (2008) 71–96, <https://doi.org/10.3322/CA.2007.0010>.
- [4] Cancer Research UK Types of lung cancer, 2019. Accessed August 23, 2021. <https://www.cancerresearchuk.org/about-cancer/lung-cancer/stages-types-grades/types>.
- [5] W.D. Travis, E. Brambilla, M. Noguchi, et al., International association for the study of lung cancer/american thoracic society/european respiratory society international multidisciplinary classification of lung adenocarcinoma, J. Thorac. Oncol. 6 (2) (2011) 244–285, <https://doi.org/10.1097/JTO.0B013E318206A221>.
- [6] M. Yotsukura, H. Asamura, N. Motoi, et al., Long-term prognosis of patients with resected adenocarcinoma in situ and minimally invasive adenocarcinoma of the lung, J. Thorac. Oncol. 16 (8) (2021) 1312–1320, <https://doi.org/10.1016/j.jtho.2021.04.007>.
- [7] K. Kamiya, Y. Hayashi, J. Douguchi, et al., Histopathological features and prognostic significance of the micropapillary pattern in lung adenocarcinoma, Mod. Pathol. 21 (8) (2008) 992–1001, <https://doi.org/10.1038/modpathol.2008.79>.
- [8] C.M. Rudin, E. Brambilla, C. Faivre-Finn, J. Sage, Small-cell lung cancer, Nat. Rev. Dis. Prim. 7 (1) (2021) 3, <https://doi.org/10.1038/S41572-020-00235-0>.
- [9] D.R. Aberle, A.M. Adams, C.D. Berg, et al., Reduced lung-cancer mortality with low-dose computed tomographic screening, N. Engl. J. Med. 365 (5) (2011) 395–409.
- [10] U. Yousaf-Khan, N. Horeweg, C. van der Aalst, K. ten Haaf, M. Oudkerk, H. de Koning, Baseline Characteristics and Mortality Outcomes of Control Group Participants and Eligible Non-Responders in the NELSON Lung Cancer Screening Study, J. Thorac. Oncol. 10 (5) (2015) 747–753, <https://doi.org/10.1097/JTO.0000000000000488>.
- [11] A.W. Blackstock, R. Govindan, Definitive chemoradiation for the treatment of locally advanced non-small-cell lung cancer, J. Clin. Oncol. 25 (26) (2007) 4146–4152, <https://doi.org/10.1200/JCO.2007.12.6581>.
- [12] N. O'Rourke, M. Roqué i Figuls, N. Farré Bernadó, F. Macbeth, Concurrent chemoradiotherapy in non-small cell lung cancer, Cochrane Database Syst. Rev. (6) (2010), <https://doi.org/10.1002/14651858.CD002140.pub3>.
- [13] S. Lantuejoul, M. Sound-Tsao, W.A. Cooper, et al., PD-L1 Testing for Lung Cancer in 2019: Perspective From the IASLC Pathology Committee, J. Thorac. Oncol. 15 (4) (2020) 499–519, <https://doi.org/10.1016/j.jtho.2019.12.107>.
- [14] J. McLaughlin, G. Han, K.A. Schalper, et al., Quantitative Assessment of the Heterogeneity of PD-L1 Expression in Non-Small-Cell Lung Cancer, JAMA Oncol. 2 (1) (2016) 46–54, <https://doi.org/10.1001/jamaoncol.2015.3638>.
- [15] L. Sholl, Molecular diagnostics of lung cancer in the clinic, Transl. Lung Cancer Res 6 (5) (2017) 560–569, <https://doi.org/10.21037/tlcr.2017.08.03>.
- [16] Velazquez E.R. Aerts HJWL, R.T.H. Leijenaar, et al., Decoding tumour phenotype by noninvasive imaging using a quantitative radiomics approach, Nat. Commun. (2014) 5, <https://doi.org/10.1038/ncomms5006>.
- [17] P. Lambin, R.T.H. Leijenaar, T.M. Deist, et al., Radiomics: the bridge between medical imaging and personalized medicine, Nat. Rev. Clin. Oncol. 14 (12) (2017) 749–762, <https://doi.org/10.1038/nrlonc.2017.141>.
- [18] I. Nwogu, J.J. Corso, Exploratory identification of image-based biomarkers for solid mass pulmonary tumors, Med. Image Comput. Comput. Assist. Interv. 11 (Pt 1) (2008) 612–619, https://doi.org/10.1007/978-3-540-85988-8_73.
- [19] E. Segal, C.B. Sirlin, C. Ooi, et al., Decoding global gene expression programs in liver cancer by noninvasive imaging, Nat. Biotechnol. 25 (6) (2007) 675–680, <https://doi.org/10.1038/nbt1306>.
- [20] P. Lambin, E. Rios-Velazquez, R. Leijenaar, et al., Radiomics: extracting more information from medical images using advanced feature analysis, Eur. J. Cancer 48 (4) (2012) 441–446, <https://doi.org/10.1016/J.EJCA.2011.11.036>.
- [21] A. Zwanenburg, M. Vallières, M.A. Abdalah, et al., The Image Biomarker Standardization Initiative: Standardized Quantitative Radiomics for High-Throughput Image-based Phenotyping, Radiology 295 (2) (2020) 328–338, <https://doi.org/10.1148/radiol.2020191145>.
- [22] J.J.M. Van Griethuysen, A. Fedorov, C. Parmar, et al., Computational radiomics system to decode the radiographic phenotype, Cancer Res 77 (21) (2017) e104–e107, <https://doi.org/10.1158/0008-5472.CAN-17-0339>.
- [23] Takashima S., Sone S., Li F., et al. Small Solitary Pulmonary Nodules (≤ 1 cm) Detected at Population-Based CT Screening for Lung Cancer: Reliable High-

- Resolution CT Features of Benign Lesions. <http://dx.doi.org/10.2214/ajr.18041800955>. 2012;180(4):955–964. doi:10.2214/AJR.180.4.1800955.
- [24] A. Snoekx, P. Reuytens, D. Desbuquoit, et al., Evaluation of the solitary pulmonary nodule: size matters, but do not ignore the power of morphology, *Insights Imaging* 9 (1) (2018) 73–86, <https://doi.org/10.1007/S13244-017-0581-2>.
- [25] Henschke C.I., Yankelevitz D.F., Mirtcheva R., McGuinness G., McCauley D., Miettinen O.S. CT Screening for Lung Cancer. <http://dx.doi.org/10.2214/ajr.17851781053>. 2012;178(5):1053–1057. doi:10.2214/AJR.178.5.1781053.
- [26] R.M. Haralick, K. Shanmugam, I. Dinstein, Textural features for image classification, *IEEE Trans. Syst. Man Cyber SMC-3* (6) (1973) 610–621, <https://doi.org/10.1109/TSMC.1973.4309314>.
- [27] A. Davis, R. Gao, N. Navin, Tumor evolution: Linear, branching, neutral or punctuated, *Biochim Biophys. Acta* 1867 (2) (2017) 151, <https://doi.org/10.1016/J.BBCAN.2017.01.003>.
- [28] Velazquez E.R. Aerts HJWL, R.T.H. Leijenaar, et al., Decoding tumour phenotype by noninvasive imaging using a quantitative radiomics approach, *Nat. Commun.* 2014 5:1 5 (1) (2014) 1–9, <https://doi.org/10.1038/ncomms5006>.
- [29] J. Zhou, J. Lu, C. Gao, et al., Predicting the response to neoadjuvant chemotherapy for breast cancer: wavelet transforming radiomics in MRI, *BMC Cancer* 20 (1) (2020), <https://doi.org/10.1186/S12885-020-6523-2>.
- [30] A. Fedorov, R. Beichel, J. Kalpathy-Cramer, et al., 3D Slicer as an image computing platform for the Quantitative Imaging Network, *Magn. Reson Imaging* 30 (9) (2012) 1323–1341, <https://doi.org/10.1016/j.mri.2012.05.001>.
- [31] L. Rinaldi, S.P. De Angelis, S. Raimondi, et al., Reproducibility of radiomic features in CT images of NSCLC patients: an integrative analysis on the impact of acquisition and reconstruction parameters, *Eur. Radio. Exp.* 6 (1) (2022) 1–13, <https://doi.org/10.1186/S41747-021-00258-6>.
- [32] Rani D.S., Rani T.S., Durga Bhavani S. Feature subset selection using consensus clustering. ICAPR 2015 - 2015 8th International Conference on Advances in Pattern Recognition. Published online February 26, 2015. doi:10.1109/ICAPR.2015.7050659.
- [33] C. Parmar, R.T.H. Leijenaar, P. Grossmann, et al., Radiomic feature clusters and Prognostic Signatures specific for Lung and Head & Neck cancer, *Sci. Rep.* 2015 5: 1 5 (1) (2015) 1–10, <https://doi.org/10.1038/srep11044>.
- [34] X. Zhang, Y. Zhang, G. Zhang, et al., Deep learning with radiomics for disease diagnosis and treatment: challenges and potential, *Front Oncol.* (2022) 12, <https://doi.org/10.3389/FONC.2022.773840>.
- [35] C. Xue, J. Yuan, G.G. Lo, et al., Radiomics feature reliability assessed by intraclass correlation coefficient: a systematic review, *Quant. Imaging Med Surg.* 11 (10) (2021) 4431, <https://doi.org/10.21037/QIMS-21-86>.
- [36] G.S. Collins, J.B. Reitsma, D.G. Altman, K.G.M. Moons, Transparent reporting of a multivariable prediction model for individual prognosis or diagnosis (TRIPOD): The TRIPOD Statement, *BMC Med* 13 (1) (2015) 1–10, <https://doi.org/10.1186/S12916-014-0241-Z>.
- [37] H. Horng, A. Singh, B. Yousefi, et al., Generalized ComBat harmonization methods for radiomic features with multi-modal distributions and multiple batch effects, *Sci. Rep.* 2022 12:1 12 (1) (2022) 1–12, <https://doi.org/10.1038/s41598-022-08412-9>.
- [38] R.N. Mahon, M. Ghita, G.D. Hugo, E. Weiss, ComBat harmonization for radiomic features in independent phantom and lung cancer patient computed tomography datasets, *Phys. Med Biol.* 65 (1) (2020), 015010, <https://doi.org/10.1088/1361-6560/AB6177>.
- [39] S.H. Hawkins, J.N. Korecki, Y. Balagurunathan, et al., Predicting outcomes of nonsmall cell lung cancer using CT image features, *IEEE Access* 2 (2014) 1418–1426, <https://doi.org/10.1109/ACCESS.2014.237335>.
- [40] Huang Y., Liu Z., He L., et al. Radiomics Signature: A Potential Biomarker for the Prediction of Disease-Free Survival in Early-Stage (I or II) Non—Small Cell Lung Cancer. <https://doi.org/10.1148/radiol.2016152234>. 2016;281(3):947–957. doi: 10.1148/RADIOL.2016152234.
- [41] Y. Moon, S.W. Sung, K.Y. Lee, J.K. Park, Clinicopathological characteristics and prognosis of non-lepidic invasive adenocarcinoma presenting as ground glass opacity nodule, *J. Thorac. Dis.* 8 (9) (2016) 2562, <https://doi.org/10.21037/JTD.2016.08.46>.
- [42] F. Nasim, T. Moua, Lung cancer in combined pulmonary fibrosis and emphysema: a large retrospective cohort analysis, *ERJ Open Res* 6 (4) (2020) 00521–02020, <https://doi.org/10.1183/23120541.00521-2020>.
- [43] D. Kawahara, N. Imano, R. Nishioka, et al., Prediction of radiation pneumonitis after definitive radiotherapy for locally advanced non-small cell lung cancer using multi-region radiomics analysis, *Sci. Rep.* 2021 11:1 11 (1) (2021) 1–9, <https://doi.org/10.1038/s41598-021-95643-x>.
- [44] L. Wu, X. Lou, N. Kong, M. Xu, C. Gao, Can quantitative peritumoral CT radiomics features predict the prognosis of patients with non-small cell lung cancer? A systematic review, *Eur. Radiol. Publ. Online* Oct. 29 (2022) 1–13, <https://doi.org/10.1007/S00330-022-09174-8>.
- [45] S. Lee, J. Jung, H. Hong, B.S. Kim, Prediction of Two-Year Recurrence-Free Survival in Operable NSCLC Patients Using Radiomic Features from Intra- and Size-Variant Peri-Tumoral Regions on Chest CT Images, *Diagn. (Basel)* (6) (2022) 12, <https://doi.org/10.3390/DIAGNOSTICS12061313>.
- [46] C.A. Owens, C.B. Peterson, C. Tang, et al., Lung tumor segmentation methods: Impact on the uncertainty of radiomics features for non-small cell lung cancer, *PLoS One* 13 (10) (2018), e0205003, <https://doi.org/10.1371/JOURNAL.PONE.0205003>.
- [47] C.F. Baumgartner, K.C. Tezcan, K. Chaitanya, et al., PhiSeg: Capturing Uncertainty in Medical Image Segmentation, in: D. Shen, T. Liu, T.M. Peters, et al. (Eds.), *Medical Image Computing and Computer Assisted Intervention – MICCAI 2019*. Springer International Publishing, 2019, pp. 119–127.
- [48] F. Isensee, P.F. Jaeger, S.A.A. Kohl, J. Petersen, K.H. Maier-Hein, nnU-Net: a self-configuring method for deep learning-based biomedical image segmentation, *Nat. Methods* 2018;15:18 (2) (2020) 203–211, <https://doi.org/10.1038/s41592-020-01008-z>.
- [49] C. Haarburger, G. Müller-Franzes, L. Weninger, C. Kuhl, D. Truhn, D. Merhof, Radiomics feature reproducibility under inter-rater variability in segmentations of CT images, *Sci. Rep.* 10 (1) (2020) 12688, <https://doi.org/10.1038/s41598-020-69534-6>.
- [50] M.A. Arshad, A. Thornton, H. Lu, et al., Discovery of pre-therapy 2-deoxy-2-(18)F-fluoro-D-glucose positron emission tomography-based radiomics classifiers of survival outcome in non-small-cell lung cancer patients, *Eur. J. Nucl. Med Mol. Imaging* 46 (2) (2019) 455–466, <https://doi.org/10.1007/s00259-018-4139-4>.
- [51] I. Rish, An empirical study of the naïve Bayes classifier, *IJCAI 2001 Workshop Empir. Methods Artif. Intell.* 3 (2001) 22.
- [52] W. Wu, C. Parmar, P. Grossmann, et al., Exploratory study to identify radiomics classifiers for lung cancer histology, *Front Oncol.* 6 (MAR) (2016) 71, <https://doi.org/10.3389/FONC.2016.00071>.
- [53] M. Avanzo, J. Stancanello, G. Pirrone, G. Sartor, Radiomics and deep learning in lung cancer, *Strahl. Onkol.* 196 (10) (2020) 879–887, <https://doi.org/10.1007/S00066-020-01625-9>.
- [54] N. Ali, D. Neagu, P. Trundle, Evaluation of k-nearest neighbour classifier performance for heterogeneous data sets, *SN Appl. Sci.* 1 (12) (2019) 1559, <https://doi.org/10.1007/s42452-019-1356-9>.
- [55] L. Breiman, Random forests, *Mach. Learn* 45 (1) (2001) 5–32, <https://doi.org/10.1023/A:1010933404324/METRICS>.
- [56] H. Wang, D. Hu, Comparison of SVM and LS-SVM for regression, *Proc. 2005 Int. Conf. Neural Netw. Brain Proc., ICNNB'05* 1 (2005) 279–283, <https://doi.org/10.1109/ICNNB.2005.1614615>.
- [57] M. Verleysen, D. François, The curse of dimensionality in data mining and time series prediction, *Lect. Notes Comput. Sci.* 3512 (2005) 758–770, https://doi.org/10.1007/11494669_9-COVER.
- [58] W. Wu, C. Parmar, P. Grossmann, et al., Exploratory Study to Identify Radiomics Classifiers for Lung Cancer Histology, *Front Oncol.* 6 (MAR) (2016), <https://doi.org/10.3389/FONC.2016.00071>.
- [59] S. Sepehri, O. Tankyevych, T. Upadhyaya, D. Visvikis, M. Hatt, C.C. Le Rest, Comparison and Fusion of Machine Learning Algorithms for Prospective Validation of PET/CT Radiomic Features Prognostic Value in Stage II-III Non-Small Cell Lung Cancer, *Diagnostics* 11 (4) (2021), <https://doi.org/10.3390/DIAGNOSTICS11040675>.
- [60] H. Abdi, L.J. Williams, Principal component analysis, *Wiley Inter. Rev. Comput. Stat.* 2 (4) (2010) 433–459, <https://doi.org/10.1002/WICS.101>.
- [61] Y. Zhang, A. Oikonomou, A. Wong, M.A. Haider, F. Khalvati, Radiomics-based prognosis analysis for non-small cell lung cancer, *Sci. Rep.* (2017) 7, <https://doi.org/10.1038/SREP46349>.
- [62] K.P. Sinaga, M.S. Yang, Unsupervised K-means clustering algorithm, *IEEE Access* 8 (2020) 80716–80727, <https://doi.org/10.1109/ACCESS.2020.2988796>.
- [63] B.F. Darst, K.C. Malecki, C.D. Engelman, Using recursive feature elimination in random forest to account for correlated variables in high dimensional data, *BMC Genet* 19 (S1) (2018) 65, <https://doi.org/10.1186/s12863-018-0633-8>.
- [64] E. Carrasquinh, J. Santinha, A. Mongolin, et al., Regularization Techniques in Radiomics: A Case Study on the Prediction of pCR in Breast Tumours and the Axilla, in: *Lecture Notes in Computer Science (Including Subseries Lecture Notes in Artificial Intelligence and Lecture Notes in Bioinformatics)*, Vol 12313, LNBI. Springer Science and Business Media Deutschland GmbH, 2020, pp. 271–281, https://doi.org/10.1007/978-3-030-63061-4_24.
- [65] H. Lu, M. Arshad, A. Thornton, et al., A mathematical-descriptor of tumor-mesoscopic-structure from computed-tomography images annotates prognostic- and molecular-phenotypes of epithelial ovarian cancer, *Nat. Commun.* 2019 10:1 10 (1) (2019) 1–11, <https://doi.org/10.1038/s41467-019-08718-9>.
- [66] M. Chen, H. Lu, S.J. Copley, et al., A Novel Radiogenomics Biomarker for Predicting Treatment Response and Pneumotoxicity from Programmed Cell Death-1 Pathway Inhibition in Non-Small Cell Lung Cancer. *J Thorac Oncol*, Published online February,, 2023, <https://doi.org/10.1016/J.JTHO.2023.01.089>.
- [67] G. Ge, J. Zhang, Feature selection methods and predictive models in CT lung cancer radiomics, *J. Appl. Clin. Med Phys.* 24 (1) (2023), e13869, <https://doi.org/10.1002/ACM2.13869>.
- [68] H. lu Cho, H.Y. Lee, E. Kim, et al., Radiomics-guided deep neural networks stratify lung adenocarcinoma prognosis from CT scans, *Commun. Biol.* 2021 4:1 4 (1) (2021) 1–12, <https://doi.org/10.1038/s42003-021-02814-7>.
- [69] Afshar P., Mohammadi A., Tyrrell P.N., et al. DRTOP: deep learning-based radiomics for the time-to-event outcome prediction in lung cancer. 2020;10: 12366. doi:10.1038/s41598-020-69106-8.
- [70] A. Hosny, H.J. Aerts, R.H. Mak, Handcrafted versus deep learning radiomics for prediction of cancer therapy response, *Lancet Digit Health* 1 (3) (2019) e106–e107, [https://doi.org/10.1016/S2589-7500\(19\)30062-7](https://doi.org/10.1016/S2589-7500(19)30062-7).
- [71] B. Lou, S. Doken, T. Zhuang, et al., An image-based deep learning framework for individualising radiotherapy dose: a retrospective analysis of outcome prediction, *Lancet Digit Health* 1 (3) (2019) e136–e147, [https://doi.org/10.1016/S2589-7500\(19\)30058-5](https://doi.org/10.1016/S2589-7500(19)30058-5).
- [72] A. Hosny, C. Parmar, T.P. Coroller, et al., Deep learning for lung cancer prognostication: A retrospective multi-cohort radiomics study, *PLoS Med* 15 (11) (2018), e1002711, <https://doi.org/10.1371/JOURNAL.PMED.1002711>.

- [73] S. Bakr, O. Gevaert, S. Echegaray, et al., A radiogenomic dataset of non-small cell lung cancer, *Sci. Data* 5 (2018), 180202, <https://doi.org/10.1038/sdata.2018.202>.
- [74] N.J. Edwards, M. Oberti, R.R. Thangudu, et al., The CPTAC Data Portal: A Resource for Cancer Proteomics Research, *J. Proteome Res* 14 (6) (2015) 2707–2713, <https://doi.org/10.1021/pr501254j>.
- [75] P.S. Hammerman, D. Voet, M.S. Lawrence, et al., Comprehensive genomic characterization of squamous cell lung cancers, *Nat.* 2012 489:7417 489 (7417) (2012) 519–525, <https://doi.org/10.1038/nature11404>.
- [76] Y.H. Zhang, Y. Lu, H. Lu, Y.M. Zhou, Development of a survival prognostic model for non-small cell lung cancer, *Front Oncol.* 10 (2020) 362, <https://doi.org/10.3389/FONC.2020.00362>.
- [77] J.R. Ferreira Junior, M. Koenigkam-Santos, F.E.G. Cipriano, A.T. Fabro, P.M. de Azevedo-Marques, Radiomics-based features for pattern recognition of lung cancer histopathology and metastases, *Comput. Methods Prog. Biomed.* 159 (2018) 23–30, <https://doi.org/10.1016/J.CMPB.2018.02.015>.
- [78] P. Hao, B.Y. Deng, C.T. Huang, et al., Predicting anaplastic lymphoma kinase rearrangement status in patients with non-small cell lung cancer using a machine learning algorithm that combines clinical features and CT images, *Front Oncol.* (2022) 12, <https://doi.org/10.3389/FONC.2022.994285>.
- [79] J.R. Kratz, D.M. Jablons, Genomic Prognostic Models in Early-Stage Lung Cancer, *Clin. Lung Cancer* 10 (3) (2009) 151–157, <https://doi.org/10.3816/CLC.2009.N.021>.
- [80] M. Skrzypski, E. Jassem, M. Taron, et al., Three-gene expression signature predicts survival in early-stage squamous cell carcinoma of the lung, *Clin. Cancer Res* 14 (15) (2008) 4794–4799, <https://doi.org/10.1158/1078-0432.CCR-08-0576>.
- [81] C.E. Reed, A. Graham, R.S. Hoda, et al., A simple two-gene prognostic model for adenocarcinoma of the lung, *J. Thorac. Cardiovasc Surg.* 135 (3) (2008) 627–634, <https://doi.org/10.1016/J.JTCVS.2007.10.058>.
- [82] L. Shui, H. Ren, X. Yang, et al., The era of radiogenomics in precision medicine: an emerging approach to support diagnosis, treatment decisions, and prognostication in oncology, *Front Oncol.* 10 (2021) 3195, <https://doi.org/10.3389/FONC.2020.570465/BIBTEX>.
- [83] G. Rossi, E. Barabino, A. Fedeli, et al., Radiomic Detection of EGFR Mutations in NSCLC, *Cancer Res* 81 (3) (2021) 724–731, <https://doi.org/10.1158/0008-5472.CAN-20-0999>.
- [84] L. Song, Z. Zhu, L. Mao, et al., Clinical, Conventional CT and Radiomic Feature-Based Machine Learning Models for Predicting ALK Rearrangement Status in Lung Adenocarcinoma Patients, *Front Oncol.* 10 (2020) 369, <https://doi.org/10.3389/FONC.2020.00369>.
- [85] R. Sun, N. Sundahl, M. Hecht, et al., Radiomics to predict outcomes and abscopal response of patients with cancer treated with immunotherapy combined with radiotherapy using a validated signature of CD8 cells, *J. Immunother. Cancer* 8 (2) (2020), e001429, <https://doi.org/10.1136/JITC-2020-001429>.
- [86] R. Sun, E.J. Limkin, M. Vakalopoulou, et al., A radiomics approach to assess tumour-infiltrating CD8 cells and response to anti-PD-1 or anti-PD-L1 immunotherapy: an imaging biomarker, retrospective multicohort study, *Lancet Oncol.* 19 (9) (2018) 1180–1191, [https://doi.org/10.1016/S1470-2045\(18\)30413-3](https://doi.org/10.1016/S1470-2045(18)30413-3).
- [87] S. Hendry, D.J. Byrne, G.M. Wright, et al., Comparison of Four PD-L1 Immunohistochemical Assays in Lung Cancer, Published online, 2018, <https://doi.org/10.1016/j.jtho.2017.11.112>.
- [88] M.F. Senosain, P.P. Mission, Intratumor Heterogeneity in Early Lung Adenocarcinoma, *Front Oncol.* 10 (2020) 349, <https://doi.org/10.3389/FONC.2020.00349>.
- [89] J. Qian, S. Olbrecht, B. Boeckx, et al., A pan-cancer blueprint of the heterogeneous tumor microenvironment revealed by single-cell profiling, *Cell Res.* 2020 30:9 30 (9) (2020) 745–762, <https://doi.org/10.1038/s41422-020-0355-0>.
- [90] J. Qi, Z. Deng, G. Sun, S. Qian, L. Liu, B. Xu, One-step algorithm for fast-track localization and multi-category classification of histological subtypes in lung cancer, *Eur. J. Radio.* (2022) 154, <https://doi.org/10.1016/J.EJRAD.2022.110443>.
- [91] L.W. Chen, S.M. Yang, H.J. Wang, et al., Prediction of micropapillary and solid pattern in lung adenocarcinoma using radiomic values extracted from near-pure histopathological subtypes, *Eur. Radio.* 31 (7) (2021) 5127–5138, <https://doi.org/10.1007/S00330-020-07570-6>.
- [92] R. Perez-Johnston, J.A. Araujo-Filho, J.G. Connolly, et al., CT-based Radiogenomic Analysis of Clinical Stage I Lung Adenocarcinoma with Histopathologic Features and Oncologic Outcomes, *Radiology* 303 (3) (2022) 664–672, <https://doi.org/10.1148/RADIOL.211582>.
- [93] L. Chen, L. Yu, X. Li, Z. Tian, X. Lin, Value of CT Radiomics and Clinical Features in Predicting Bone Metastases in Patients with NSCLC, *Contrast Media Mol. Imaging* (2022) 2022, <https://doi.org/10.1155/2022/7642511>.
- [94] X. Xu, L. Huang, J. Chen, et al., Application of radiomics signature captured from pretreatment thoracic CT to predict brain metastases in stage III/IV ALK-positive non-small cell lung cancer patients, *J. Thorac. Dis.* 11 (11) (2019) 4516, <https://doi.org/10.21037/JTD.2019.11.01>.
- [95] F. Cucchiara, I. Petrini, C. Romei, et al., Combining liquid biopsy and radiomics for personalized treatment of lung cancer patients, *State Art. N. Perspect. Pharm. Res.* (2021) 169, <https://doi.org/10.1016/J.JPHRS.2021.105643>.
- [96] S. Li, C. Ding, H. Zhang, J. Song, L. Wu, Radiomics for the prediction of EGFR mutation subtypes in non-small cell lung cancer, *Med Phys.* 46 (10) (2019) 4545–4552, <https://doi.org/10.1002/MP.13747>.
- [97] L. Zhang, B. Chen, X. Liu, et al., Quantitative biomarkers for prediction of epidermal growth factor receptor mutation in non-small cell lung cancer, *Transl. Oncol.* 11 (1) (2018) 94–101, <https://doi.org/10.1016/J.TRANON.2017.10.012>.
- [98] Y. Liu, J. Kim, Y. Balagurunathan, et al., Radiomic Features Are Associated With EGFR Mutation Status in Lung Adenocarcinomas, *e6, Clin. Lung Cancer* 17 (5) (2016) 441–448, <https://doi.org/10.1016/J.CLLC.2016.02.001>.
- [99] W. Tu, G. Sun, L. Fan, et al., Radiomics signature: A potential and incremental predictor for EGFR mutation status in NSCLC patients, comparison with CT morphology, *Lung Cancer* 132 (2019) 28–35, <https://doi.org/10.1016/J.LUNGCAN.2019.03.025>.
- [100] B. Cheng, H. Deng, Y. Zhao, et al., Predicting EGFR mutation status in lung adenocarcinoma presenting as ground-glass opacity: utilizing radiomics model in clinical translation, *Eur. Radio.* 32 (9) (2022) 5869–5879, <https://doi.org/10.1007/s00330-022-08673-y>.
- [101] G.J. Riely, W. Pao, D.K. Pham, et al., Clinical course of patients with non-small cell lung cancer and epidermal growth factor receptor exon 19 and exon 21 mutations treated with gefitinib or erlotinib, *Clin. Cancer Res* 12 (3 Pt 1) (2006) 839–844, <https://doi.org/10.1158/1078-0432.CCR-05-1846>.
- [102] X. Yang, C. Fang, C. Li, et al., Can CT Radiomics Detect Acquired T790M Mutation and Predict Prognosis in Advanced Lung Adenocarcinoma With Progression After First- or Second-Generation EGFR TKIs, *Front Oncol.* (2022) 12, <https://doi.org/10.3389/FONC.2022.904983>.
- [103] C. Chang, X. Sun, G. Wang, et al., A Machine Learning Model Based on PET/CT Radiomics and Clinical Characteristics Predicts ALK Rearrangement Status in Lung Adenocarcinoma, *Front Oncol.* 11 (2021) 1, <https://doi.org/10.3389/FONC.2021.603882/FULL>.
- [104] P. Tian, B. He, W. Mu, et al., Assessing PD-L1 expression in non-small cell lung cancer and predicting responses to immune checkpoint inhibitors using deep learning on computed tomography images, *Theranostics* 11 (5) (2021) 2098, <https://doi.org/10.7150/THNO.48027>.
- [105] T.S.K. Mok, Y.L. Wu, I. Kudaba, et al., Pembrolizumab versus chemotherapy for previously untreated, PD-L1-expressing, locally advanced or metastatic non-small-cell lung cancer (KEYNOTE-042): a randomised, open-label, controlled, phase 3 trial, *Lancet* 393 (10183) (2019) 1819–1830, [https://doi.org/10.1016/S0140-6736\(18\)32409-7](https://doi.org/10.1016/S0140-6736(18)32409-7).
- [106] M.D. Hellmann, L. Paz-Ares, R. Bernabe Caro, et al., Nivolumab plus Ipilimumab in Advanced Non-Small-Cell Lung Cancer, *N. Engl. J. Med.* 381 (21) (2019) 2020–2031, <https://doi.org/10.1056/NEJMoa1910231>.
- [107] C. Wang, J. Ma, J. Shao, et al., Non-Invasive Measurement Using Deep Learning Algorithm Based on Multi-Source Features Fusion to Predict PD-L1 Expression and Survival in NSCLC, *Front Immunol.* (2022) 13, <https://doi.org/10.3389/FIMMU.2022.828560>.
- [108] I. Tsimafeyeu, E. Imanitov, L. Zavalishina, et al., Agreement between PD-L1 immunohistochemistry assays and polymerase chain reaction in non-small cell lung cancer: CLOVER comparison study, *Sci. Rep.* 10 (1) (2020) 3928, <https://doi.org/10.1038/s41598-020-06950-2>.
- [109] J. Shao, J. Ma, S. Zhang, et al., Radiogenomic System for Non-Invasive Identification of Multiple Actionable Mutations and PD-L1 Expression in Non-Small Cell Lung Cancer Based on CT Images, *Cancers (Basel)* 14 (19) (2022), <https://doi.org/10.3390/CANCERS14194823>.
- [110] Q. Chen, J.J. Shao, T. Xue, et al., Intratumoral and peritumoral radiomics nomograms for the preoperative prediction of lymphovascular invasion and overall survival in non-small cell lung cancer, *Eur. Radiol. Publ. Online* (2022), <https://doi.org/10.1007/S00330-022-09109-3>.
- [111] P. Forouzannezhad, D. Maes, D.S. Hippé, et al., Multitask Learning Radiomics on Longitudinal Imaging to Predict Survival Outcomes following Risk-Adaptive Chemoradiation for Non-Small Cell Lung Cancer, *Cancers (Basel)* 14 (5) (2022), <https://doi.org/10.3390/CANCERS14051228>.
- [112] S. Hindocha, T.G. Charlton, K. Linton-Reid, et al., Gross tumour volume radiomics for prognostication of recurrence & death following radical radiotherapy for NSCLC, *NPJ Precis Oncol.* 6 (1) (2022), <https://doi.org/10.1038/S41698-022-00322-3>.
- [113] N. Chen, M. bin, Xiong, R. Zhou, et al., CT radiomics-based long-term survival prediction for locally advanced non-small cell lung cancer patients treated with concurrent chemoradiotherapy using features from tumor and tumor organismal environment, *Radiat. Oncol.* 17 (1) (2022), <https://doi.org/10.1186/S13014-022-02136-W>.
- [114] H. Kim, C.M. Park, B. Keam, et al., The prognostic value of CT radiomic features for patients with pulmonary adenocarcinoma treated with EGFR tyrosine kinase inhibitors, *PLoS One* 12 (11) (2017), <https://doi.org/10.1371/JOURNAL.PONE.0187500>.
- [115] K. Jazieh, M. Khorrami, A. Saad, et al., Novel imaging biomarkers predict outcomes in stage III unresectable non-small cell lung cancer treated with chemoradiation and durvalumab, *J. Immunother. Cancer* 10 (3) (2022), <https://doi.org/10.1136/JITC-2021-003778>.
- [116] K.H. Kim, J. Kim, H. Park, et al., Parallel comparison and combining effect of radiomic and emerging genomic data for prognostic stratification of non-small cell lung carcinoma patients, *Thorac. Cancer* 11 (9) (2020) 2542–2551, <https://doi.org/10.1111/1759-7714.13568>.
- [117] K.J. Lafata, J.C. Hong, R. Geng, et al., Association of pre-treatment radiomic features with lung cancer recurrence following stereotactic body radiation therapy, *Phys. Med. Biol.* 64 (2) (2019), 025007, <https://doi.org/10.1088/1361-6560/AA5A55>.
- [118] G. Dissaux, D. Visvikis, R. Daano, et al., Pretreatment 18F-FDG PET/CT Radiomics Predict Local Recurrence in Patients Treated with Stereotactic Body Radiotherapy

- for Early-Stage Non-Small Cell Lung Cancer: A Multicentric Study, *J. Nucl. Med.* 61 (6) (2020) 814–820, <https://doi.org/10.2967/JNNUED.119.228106>.
- [119] R. Chang, S. Qi, Y. Zuo, et al., Predicting chemotherapy response in non-small-cell lung cancer via computed tomography radiomic features: Peritumoral, intratumoral, or combined, *Front Oncol.* (2022) 12, <https://doi.org/10.3389/FONC.2022.915835>.
- [120] H. Wei, F. Yang, Z. Liu, et al., Application of computed tomography-based radiomics signature analysis in the prediction of the response of small cell lung cancer patients to first-line chemotherapy, *Exp. Ther. Med* 17 (5) (2019), <https://doi.org/10.3892/ETM.2019.7357>.
- [121] C. Yang, W. Chen, G. Gong, Z. Li, Q. Qiu, Y. Yin, Application of CT radiomics features to predict the EGFR mutation status and therapeutic sensitivity to TKIs of advanced lung adenocarcinoma, *Transl. Cancer Res* 9 (11) (2020) 6683, <https://doi.org/10.21037/TCR-20-1216>.
- [122] S. Trebeschi, S.G. Drago, N.J. Birkbak, et al., Predicting response to cancer immunotherapy using noninvasive radiomic biomarkers, *Ann. Oncol.* 30 (6) (2019) 998–1004, <https://doi.org/10.1093/ANNONC/MDZ108>.
- [123] A. Moran, M.E. Daly, S.S.F. Yip, T. Yamamoto, Radiomics-based Assessment of Radiation-induced Lung Injury After Stereotactic Body Radiotherapy, *Clin. Lung Cancer* 18 (6) (2017) e425–e431, <https://doi.org/10.1016/J.CLLC.2017.05.014>.
- [124] Y. Huang, A. Feng, Y. Lin, et al., Radiation pneumonitis prediction after stereotactic body radiation therapy based on 3D dose distribution: dosimetrics and/or deep learning-based radiomics features, *Radiat. Oncol.* 17 (1) (2022), <https://doi.org/10.1186/S13014-022-02154-8>.
- [125] S.A. Matteson, D.A. Palma, C. Johnson, et al., Detection of local cancer recurrence after stereotactic ablative radiation therapy for lung cancer: physician performance versus radiomic assessment, *Int J. Radiat. Oncol. Biol. Phys.* 94 (5) (2016) 1121–1128, <https://doi.org/10.1016/J.IJROBP.2015.12.369>.
- [126] A. Sinjab, G. Han, W. Treekitkarnmongkol, et al., Resolving the spatial and cellular architecture of lung adenocarcinoma by multiregion single-cell sequencing, *Cancer Discov* 11 (10) (2021) 2506–2523, <https://doi.org/10.1158/2159-8290.CD-20-1285>.
- [127] C.M. Lovly, A.K.S. Salama, R. Salgia, Tumor heterogeneity and therapeutic resistance, *Am. Soc. Clin. Oncol. Educ. Book* 35 (36) (2016) e585–e593, https://doi.org/10.1200/EDBK_158808.
- [128] Z. Hu, Z. Li, Z. Ma, C. Curtis, Multi-cancer analysis of clonality and the timing of systemic spread in paired primary tumors and metastases, *Nat. Genet.* 2020 52:7 52 (7) (2020) 701–708, <https://doi.org/10.1038/s41588-020-0628-z>.
- [129] H. Lu, P. Cunnea, K. Nixon, N. Rinne, E.O. Aboagye, C. Fotopoulou, Discovery of a biomarker candidate for surgical stratification in high-grade serous ovarian cancer, *Br. J. Cancer* 124 (7) (2021) 1286–1293, <https://doi.org/10.1038/s41416-020-01252-2>.
- [130] I. Tunali, Y. Tan, J.E. Gray, et al., Hypoxia-related radiomics and immunotherapy response: A multicohort study of non-small cell lung cancer, *JNCI Cancer Spectr.* 5 (4) (2021) kab048.
- [131] B. Muz, P. de la Puente, F. Azab, A.K. Azab, The role of hypoxia in cancer progression, angiogenesis, metastasis, and resistance to therapy, *Hypoxia (Auckl.)* 3 (2015) 83, <https://doi.org/10.2147/HP.S93413>.
- [132] J. Jiménez-Sánchez, J.J. Bosque, G.A. Jiménez Londoño, et al., Evolutionary dynamics at the tumor edge reveal metabolic imaging biomarkers, *Proc. Natl. Acad. Sci. USA* 118 (6) (2021), e2018110118, <https://doi.org/10.1073/pnas.2018110118>.
- [133] M.R. Chetan, F. v Gleeson, Radiomics in predicting treatment response in non-small-cell lung cancer: current status, challenges and future perspectives, *Eur. Radio.* 31 (2) (2021) 1049–1058, <https://doi.org/10.1007/S00330-020-07141-9>.
- [134] M. Rodríguez Plá, D. Dualde Beltrán, E. Ferrer Albiach, Immune Checkpoints Inhibitors and SRS/SBRT Synergy in Metastatic Non-Small-Cell Lung Cancer and Melanoma: A Systematic Review, *Int J. Mol. Sci.* 22 (21) (2021), <https://doi.org/10.3390/IJMS222111621>.
- [135] N. Haratake, T. Seto, NTRK fusion-positive non-small-cell lung cancer: the diagnosis and targeted therapy, *Clin. Lung Cancer* 22 (1) (2021) 1–5, <https://doi.org/10.1016/J.CLLC.2020.10.013>.
- [136] S. Puri, M. Shafique, Combination checkpoint inhibitors for treatment of non-small-cell lung cancer: an update on dual anti-CTLA-4 and anti-PD-1/PD-L1 therapies, *Drugs Context* (2020) 9, <https://doi.org/10.7573/DIC.2019-9-2>.
- [137] F. Zhong, Z. Liu, B. Wang, et al., A predictive model to differentiate between second primary lung cancers and pulmonary metastasis, *Acad. Radio.* 29 (2022) S137–S144, <https://doi.org/10.1016/j.acra.2021.05.015>.
- [138] F. Cucchiara, M. del Re, S. Valleggi, et al., Integrating Liquid Biopsy and Radiomics to Monitor Clonal Heterogeneity of EGFR-Positive Non-Small Cell Lung Cancer, *Front Oncol.* (2020) 10, <https://doi.org/10.3389/FONC.2020.593831>.
- [139] L. Shi, Y. Rong, M. Daly, et al., Cone-beam computed tomography-based delta-radiomics for early response assessment in radiotherapy for locally advanced lung cancer, *Phys. Med Biol.* 65 (1) (2020), <https://doi.org/10.1088/1361-6560/AB3247>.
- [140] V. Nardone, A. Reginelli, R. Grassi, et al., Delta radiomics: a systematic review, *Radiol. Med.* 126 (12) (2021) 1571–1583, <https://doi.org/10.1007/S11547-021-01436-7>.
- [141] M. Bogowicz, A. Jochems, T.M. Deist, et al., Privacy-preserving distributed learning of radiomics to predict overall survival and HPV status in head and neck cancer, *Sci. Rep.* 10 (1) (2020) 4542, <https://doi.org/10.1038/s41598-020-61297-4>.
- [142] S. Warnat-Herresthal, H. Schultze, K.L. Shastry, et al., Swarm learning for decentralized and confidential clinical machine learning, *Nature* 594 (7862) (2021) 265–270, <https://doi.org/10.1038/s41586-021-03583-3>.